이학박사 학위논문

Optical Quantum Teleportation over a Lossy Environment

손실이 일어나는 환경하에서의 광학적 양자 텔레포테이션

2017년 2월

서울대학교 대학원
물리·천문학부
김 호 용

Optical Quantum Teleportation over a Lossy Environment

Hoyong Kim

Supervised by

Associate Professor **Hyunseok Jeong**

A Dissertation

Submitted to the Faculty of

Seoul National University

in Partial Fulfillment of

the Requirements for the Degree of

Doctor of Philosophy

February 2017

Department of Physics and Astronomy

The Graduate School

Seoul National University

Abstract

Optical Quantum Teleportation over a Lossy Environment

Hoyong Kim
Department of Physics and Astronomy
The Graduate School
Seoul National University

The purpose of this thesis is to investigate the effects of photon losses which occur during the process of quantum teleportation using optical qubits. The channel state which is used as a resource for quantum teleportation is affected by decoherence while being distributed between two distant parties. Using different types of optical qubits, we analyze the performance of quantum teleportation under photon loss effects.

We introduce three different types of optical qubits. One is qubits using the vacuum and single-photon states, another is polarized single-photon qubits, and the third is coherent-state qubits. We compare information transfer efficiencies of quantum teleportation and direct transmission under photon loss effects using these different types of optical qubits. Quantum teleportation always outperforms the direct transmission for qubits using the vacuum

and single-photon states and polarized single-photon qubits. In the case of coherent-state qubits, the region where quantum teleportation outperforms the direct transmission varies according to the amplitude of coherent-state qubits. We also find that qubits using the vacuum and single-photon states are the most efficient ones among three different types of optical qubits.

In addition to above-mentioned optical qubits, two different types of optical hybrid qubits are also considered. They are the hybrid of a qubit of the vacuum and the single-photon and a coherent state-qubit, and the hybrid of a polarized single-photon qubit and a coherent-state qubit. We compare two different types of hybrid qubits for quantum teleportation under photon loss effects. It is shown that the hybrid of a qubit of the vacuum and the single-photon and a coherent-state qubit always outperforms the hybrid of a polarized single-photon qubit and a coherent-state qubit.

Keywords : Quantum teleportation, Quantum information processing, Quantum optics, Decoherence

Student Number : 2011-20399

Contents

List of Figures

Chapter 1

Introduction

Information theory should follow the laws of physics because information is basically encoded in certain characteristics of physical objects. Traditional classical information theory is based on the laws of classical physics, which is to hold approximately in the macroscopic world. However our world, especially in the microscopic world, is essentially governed by quantum mechanics, so quantum information theory which is the combination of quantum mechanics and information theory is needed. Two important features of quantum information theory are quantum superposition and quantum entanglement. The basic unit of quantum information theory is 'qubit', which is a compound word of quantum and bit [1]. In classical information theory, one classical bit can have a definite value of 0 or 1, while a qubit in quantum information theory can be any superposition of 0 and 1 [2]. Quantum entanglement is the correlation between quantum systems which is beyond classical correlation [3, 4].

Quantum infomation processing offers many advantages over classical information processing. The idea of quantum computers was suggested by Feynman to simulate quantum mechanical systems [5]. Quantum computers can perform many computations simultaneously, which is known as quantum

parallelism. There are quantum algorithms, such as Shor's quantum factoring algorithm [6] and Grover's quantum search algorithm [7], which run faster than classical algorithms by utilizing quantum parallelism. Quantum key distribution such as BB84 protocol [8] enables two parties to share a secret key for secure communication.

Using quantum entanglement, Bennett *et al.* proposed a protocol to transfer quantum information to a distant place, which is called quantum teleportation [9]. Quantum teleportation is useful for quantum communication and quantum computing. It can be generalized to entanglement swapping [10] required for quantum repeaters [11], or quantum gate teleportation which is a central element of quantum information processing [12]. Obviously, it is also possible to transmit the physical object carrying quantum information directly. The difference between quantum teleportation and direct transmission is that quantum teleportation only transfers the information without transmitting the physical object carrying quantum information. Quantum teleportation may be a better candidate for quantum information transfer when the direct transmission is unreliable due to decoherence effects [13].

One of the most prominent candidates for quantum information processing is optical systems, since they naturally integrate quantum computation and quantum communication [14, 15]. It was shown that efficient quantum computation with linear optics is possible [16]. In optical quantum information processing, the basis of optical qubits, 0 and 1, should correspond some physical degrees of freedom of photons. One possible choice is dual-rail en-

codings which utilize two distinct optical modes of a single photon, such as horizontally and vertically polarized modes, to represent optical qubits [16]. Alternatively, single-rail encodings only use one optical mode, and encode information in two distinct states of a single optical mode, such as the vacuum and single-photon states [17] or two different coherent states [18, 19].

In this thesis, we investigate the performance of optical quantum teleportation in the presence of decoherence, particularly photon loss effects. In chapter 2, we review the process of quantum teleportation and detailed quantum teleportation schemes for various types of optical qubits. In chapter 3, we compare three different types of optical qubits for quantum teleportation and direct transmission under photon loss effects. We also analyze the efficiencies of quantum teleportation using two different types of optical hybrid qubits under photon loss effects in chapter 4. We conclude in chapter 5 with a summary of all results.

This thesis is based on the following publications:

1. H. Kim, J. Park, and H. Jeong, "Transfer of different types of optical qubits over a lossy environment," Phys. Rev. A **89**, 042303 (2014).

2. H. Kim, S.-W. Lee, and H. Jeong, "Two different types of optical hybrid qubits for teleportation in a lossy environment," Quantum Inf. Process. **15**, 4729 (2016).

Chapter 2

Quantum teleportation

2.1 Concept of quantum teleportation

Quantum teleportation allows the transfer of an unknown quantum state without directly transmitting the quantum state itself. It requires a previously shared entangled state and a classical communication channel between the sender and the receiver. The process of quantum teleportation is illustrated in Fig. 1. Assume that the sender, Alice, want to teleport an unkown qubit,

$$|\psi\rangle = \mu|0_L\rangle + \nu|1_L\rangle, \tag{2.1}$$

to the receiver, Bob. Here, $|0_L\rangle$ and $|1_L\rangle$ represent the logical 0 and 1 states, respectively, which form a qubit basis. The normalization condition $|\mu|^2 + |\nu|^2 = 1$ also should be met.

To implement quantum teleportation, Alice and Bob share one of the maximally entangled state,

$$|\Psi_L^-\rangle = \frac{1}{\sqrt{2}}(|0_L\rangle|1_L\rangle - |1_L\rangle|0_L\rangle). \tag{2.2}$$

The total product state of the unknown input state and the entangled channel

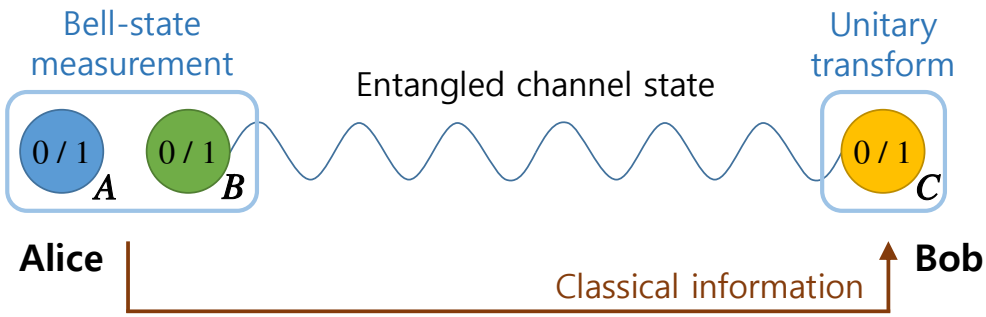

Figure 1: Standard scheme of quantum teleportation. The mode A represents the unknown input state, and the modes B and C represent the entangled channel state shared by Alice and Bob.

state can be written as

$$
\begin{aligned}
|\psi\rangle_A|\Psi_L^-\rangle_{BC} &= (\mu|0_L\rangle_A + \nu|1_L\rangle_A)\frac{1}{\sqrt{2}}(|0_L\rangle_B|1_L\rangle_C - |1_L\rangle_B|0_L\rangle_C) \\
&= \frac{1}{2}[-|\Phi_L^+\rangle_{AB}(\nu|0_L\rangle_C - \mu|1_L\rangle_C) + |\Phi_L^-\rangle_{AB}(\nu|0_L\rangle_C + \mu|1_L\rangle_C) \\
&\quad - |\Psi_L^+\rangle_{AB}(\mu|0_L\rangle_C - \nu|1_L\rangle_C) - |\Psi_L^-\rangle_{AB}(\mu|0_L\rangle_C + \nu|1_L\rangle_C)] \\
&= \frac{1}{2}[|\Phi_L^+\rangle_{AB}\hat{X}\hat{Z}|\psi\rangle_C + |\Phi_L^-\rangle_{AB}\hat{X}|\psi\rangle_C - |\Psi_L^+\rangle_{AB}\hat{Z}|\psi\rangle_C \\
&\quad - |\Psi_L^-\rangle_{AB}|\psi\rangle_C], \qquad (2.3)
\end{aligned}
$$

with the Bell states

$$|\Phi_L^\pm\rangle = \frac{1}{\sqrt{2}}(|0_L\rangle|0_L\rangle \pm |1_L\rangle|1_L\rangle), \qquad (2.4)$$

$$|\Psi_L^\pm\rangle = \frac{1}{\sqrt{2}}(|0_L\rangle|1_L\rangle \pm |1_L\rangle|0_L\rangle), \qquad (2.5)$$

and $\hat{X}$ and $\hat{Z}$ represent the Pauli operators applied on the mode C as

$$\begin{aligned} \hat{X}|0_L\rangle &= |1_L\rangle, & \hat{X}|1_L\rangle &= |0_L\rangle, \\ \hat{Z}|0_L\rangle &= |0_L\rangle, & \hat{Z}|1_L\rangle &= -|1_L\rangle, \end{aligned} \tag{2.6}$$

where the modes A and B belong to Alice and the mode C belongs to Bob.

Alice performs the Bell-state measurement as a joint measurement for the input state (mode A) and her part of the entangled channel state (mode B) to discriminate between the four Bell states $|\Phi_L^{\pm}\rangle$ and $|\Psi_L^{\pm}\rangle$. After the Bell-state measurement, Alice sends her measurement result to Bob through the classical communication channel. Bob should apply an appropriate unitary transform on his part of the entangled channel state (mode C) according to Alice's measurement results as

$$\begin{aligned} \Phi_L^+ &\rightarrow \hat{X}\hat{Z}, & \Phi_L^- &\rightarrow \hat{X}, \\ \Psi_L^+ &\rightarrow \hat{Z}, & \Psi_L^- &\rightarrow \mathbb{1}, \end{aligned} \tag{2.7}$$

to obtain the final teleported state $|\psi\rangle = \mu|0_L\rangle + \nu|1_L\rangle$.

We note that the Bell-state measurement of Alice on the modes A and B instantaneously affects the mode C, the other part of the entangled channel state, which is far away from her. However, Bob cannot realize which Pauli operator he should perform to obtain the final teleported state until the arrival of classical information of Alice's measurement result. Since classical

communication is required to complete the quantum teleportation protocol, it cannot be used as superluminal communication.

2.2 Efficiency of quantum teleportation

Quantum teleportation may not be carried out perfectly or successfully for some reasons. For example, the channel state may be a partially entangled state or a mixed state instead of the maximally entangled state due to imperfect generation of entanglement or decoherence. The discrimination of all four Bell states may also fail. In these cases, we can quantify the efficiency of quantum teleportation using fidelity and success probability. The fidelity quantifies similarity of the input state and the output state. It is defined by the overlap of the input state $|\psi\rangle$ and the output state ρ as

$$F = \langle\psi|\rho|\psi\rangle. \tag{2.8}$$

If the quantum teleportation is performed perfectly, the output state is the same as the input state which means the fidelity is 1. The success probability of quantum teleportation implies the success probability of the Bell-state measurement. To succeed the Bell-state measurement of quantum teleportation, Alice needs to discriminate all four Bell states $|\Phi_L^{\pm}\rangle$ and $|\Psi_L^{\pm}\rangle$. In the case of imperfect discrimination of the Bell states, the quantum teleportation can only be performed probabilistically.

One can see that the fidelity and the success probability depend on the in-

put state. Since Alice wants to teleport the unknown qubit $|\psi\rangle = \mu|0_L\rangle + \nu|1_L\rangle$, where μ and ν are arbitrary complex numbers satisfying the normalization condition, we need to average the fidelity and the success probability over all possible input states to obtain the efficiency of quantum teleportation. The average fidelity F_{avg} and the average success probability P_{avg} are

$$F_{\text{avg}} = \frac{1}{4\pi}\int_0^{2\pi}\int_0^{\pi} F(\theta,\phi)\sin\theta d\theta d\phi, \tag{2.9}$$

$$P_{\text{avg}} = \frac{1}{4\pi}\int_0^{2\pi}\int_0^{\pi} P(\theta,\phi)\sin\theta d\theta d\phi, \tag{2.10}$$

where the average is taken over the Bloch sphere of all possible input states $|\psi\rangle = \mu|0_L\rangle + \nu|1_L\rangle$ with $\mu = \cos(\theta/2)$ and $\nu = e^{i\phi}\sin(\theta/2)$, and $F(\theta,\phi)$ and $P(\theta,\phi)$ are the fidelity and the success probability of quantum teleportation using a particular input state,

$$|\psi\rangle = \cos(\theta/2)|0_L\rangle + e^{i\phi}\sin(\theta/2)|1_L\rangle. \tag{2.11}$$

To find out whether the quantum teleportation is meaningful or not, we consider the classical limit of teleportation, which means the bound of the average fidelity of teleportation when a product state is used as a channel state. If the average fidelity of quantum teleportation is above the classical limit, then we can conclude that our teleportation protocol has the benefit from nonclassical feature of the entangled channel state. It was shown that the classical limit of the average fidelity of teleportation is 2/3 [20, 21, 22]. Here,

we briefly introduce the scheme that attains the classical limit of 2/3. Alice measures the input state $|\psi\rangle = \cos(\theta/2)|0_L\rangle + e^{i\phi}\sin(\theta/2)|1_L\rangle$ along a given axis, say the z axis, and tells the measurement result to Bob classically. Bob prepares his state in $|0_L\rangle$ or $|1_L\rangle$ according to the Alice's measurement result. Alice obtains the outcome $|0_L\rangle$ with probability $\cos^2(\theta/2)$, and the outcome $|1_L\rangle$ with probability $\sin^2(\theta/2)$. Thus, the corresponding average fidelity is

$$F_{\rm cl} = \frac{1}{4\pi}\int_0^{2\pi}\int_0^{\pi}\{\cos^4(\theta/2) + \sin^4(\theta/2)\}\sin\theta d\theta d\phi = 2/3, \qquad (2.12)$$

which attains the classical limit of 2/3.

2.3 Quantum teleportation using optical qubits

In order to perform quantum teleportation, we need to choose some particular physical system to encode quantum information. We choose photons as information carriers for quantum teleportation. The teleportation protocol using optical qubits is depicted in Fig. 2. Among the optical qubits, we consider three different types of optical qubits, such as qubits using the vacuum and single-photon states, polarized single-photon qubits, and coherent-state qubits. In the following subsections, we will review the quantum teleportation schemes of each optical qubits, especially the Bell-state measurements and the Pauli operations.

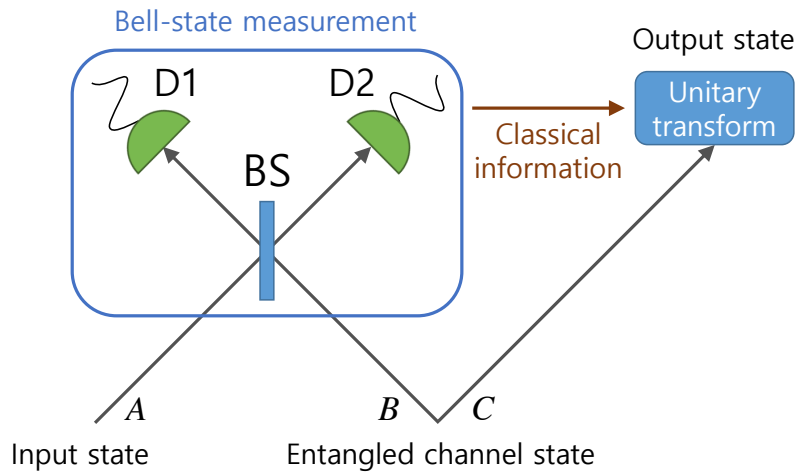

Figure 2: Optical quantum teleportation protocol and its Bell-state measurement. The Bell-state measurement of optical qubits can be performed using a 50:50 beam splitter (BS) and photon detectors (D1 and D2).

2.3.1 Qubits using the vacuum and single-photon states

Optical qubits can be constructed by the vacuum and the single-photon states.

A optical qubit using the vacuum and single-photon states is

$$|\psi_V\rangle = \mu|0\rangle + \nu|1\rangle, \tag{2.13}$$

where $|0\rangle$ and $|1\rangle$ are the vacuum and single-photon states, respectively. The Bell states of the vacuum and the single-photon states are defined as

$$|\Phi_V^{\pm}\rangle = \frac{1}{\sqrt{2}}(|0\rangle|0\rangle \pm |1\rangle|1\rangle), \tag{2.14}$$

$$|\Psi_V^{\pm}\rangle = \frac{1}{\sqrt{2}}(|0\rangle|1\rangle \pm |1\rangle|0\rangle). \tag{2.15}$$

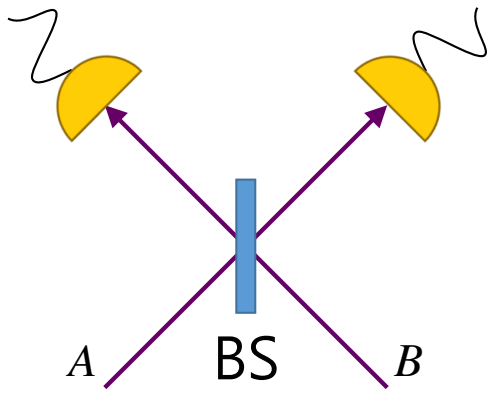

Figure 3: The Bell-state measurement for the vacuum and the single-photon states, B_V, is implemented using a 50:50 beam splitter (BS) and two single-photon detectors [23].

The Bell-state measurement for the vacuum and the single-photon states, B_V, can be performed using a 50:50 beam splitter and two single-photon detectors as shown in Fig. 3 [23]. Here, the single-photon detectors should be able to discriminate between zero, one and more than one photons. We define the 50:50 beam splitter operator as

$$U_{i,j} = e^{-\frac{\pi}{4}(a_i^\dagger a_j - a_i a_j^\dagger)}, \tag{2.16}$$

where i and j are two field modes entering the beam splitter and a_i ($a_i^\dagger$) is the annihilation (creation) operator for mode i. After the action of the beam splitter $U_{A,B}$ which is applied to qubits of modes A and B, the output states of

the Bell states of the vacuum and the single-photon states are

$$|\Psi_{\mathrm{V}}^{+}\rangle \xrightarrow{BS} |0\rangle|1\rangle, \tag{2.17}$$

$$|\Psi_{\mathrm{V}}^{-}\rangle \xrightarrow{BS} |1\rangle|0\rangle, \tag{2.18}$$

$$|\Phi_{\mathrm{V}}^{\pm}\rangle \xrightarrow{BS} \frac{1}{2}(|0\rangle|2\rangle - |2\rangle|0\rangle) \pm \frac{1}{\sqrt{2}}|0\rangle|0\rangle. \tag{2.19}$$

If one photon is detected at one detector and the other detector is silent, one can identify whether it was $|\Psi_{\mathrm{V}}^{+}\rangle$ or $|\Psi_{\mathrm{V}}^{-}\rangle$. However, if two photons are detected at one detector or both detectors are silent, we cannot find whether it was $|\Phi_{\mathrm{V}}^{+}\rangle$ or $|\Phi_{\mathrm{V}}^{-}\rangle$. Thus, the success probability of the $\mathrm{B_V}$ measurement is 1/2 [23].

The Pauli Z operation for qubits using the vacuum and single-photon states can be implemented by acting the π phase shift, $e^{i\pi\hat{a}^{\dagger}\hat{a}}$. However, the Pauli X operation for qubits using the vacuum and single-photon states can only be implemented probabilistically using nondeterministic Hadamard gate $\hat{H}$ proposed in Ref. [17] and the π phase shifter as $\hat{X} = \hat{H}\hat{Z}\hat{H}$.

2.3.2 Polarized single-photon qubits

Polarized single-photon qubits utilize horizontally polarized state $|H\rangle$, and vertically polarized state $|V\rangle$, as a qubit basis. A polarized single-photon qubit is

$$|\psi_{\mathrm{P}}\rangle = \mu|H\rangle + \nu|V\rangle, \tag{2.20}$$

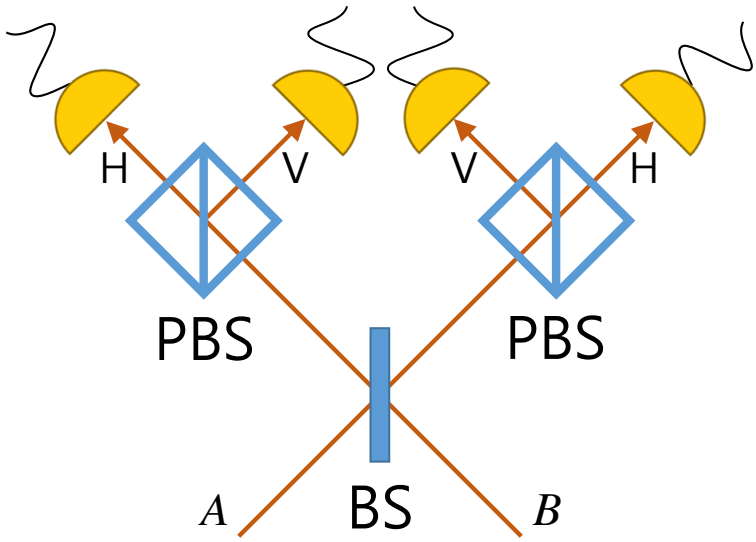

Figure 4: The Bell-state measurement for the polarized single-photon states, B_P, is performed using a 50:50 beam splitter (BS), two polarizing beam splitters (PBS), and four single-photon detectors [24].

and the Bell states of polarized single-photon states are

$$|\Phi_P^{\pm}\rangle = \frac{1}{\sqrt{2}}(|H\rangle|H\rangle \pm |V\rangle|V\rangle), \tag{2.21}$$

$$|\Psi_P^{\pm}\rangle = \frac{1}{\sqrt{2}}(|H\rangle|V\rangle \pm |V\rangle|H\rangle). \tag{2.22}$$

The Bell-state measurement for the polarized single-photon states, B_P, can be performed using a 50:50 beam splitter, two polarizing beam splitters and four single-photon detectors as shown in Fig. 4 [24]. The polarizing beam splitters are used to distinguish between the horizontally and vertically polarized states. The horizontally polarized states are always transmitted, while the vertically polarized states are always reflected. By applying the beam splitter

$U_{A,B}$, the Bell states of the polarized single-photon states are transformed as

$$|\Psi_{\mathrm{P}}^{+}\rangle \xrightarrow{BS} \frac{1}{\sqrt{2}}(|HV\rangle|0\rangle - |0\rangle|HV\rangle), \tag{2.23}$$

$$|\Psi_{\mathrm{P}}^{-}\rangle \xrightarrow{BS} \frac{1}{\sqrt{2}}(|H\rangle|V\rangle - |V\rangle|H\rangle), \tag{2.24}$$

$$|\Phi_{\mathrm{P}}^{\pm}\rangle \xrightarrow{BS} \frac{1}{2}(|HH\rangle|0\rangle - |0\rangle|HH\rangle) \pm \frac{1}{2}(|VV\rangle|0\rangle - |0\rangle|VV\rangle). \tag{2.25}$$

By detecting one photon at one detector and one photon at another detector, two ($|\Psi_{\mathrm{P}}^{+}\rangle$ and $|\Psi_{\mathrm{P}}^{-}\rangle$) of the four Bell states can be discriminated. If two photons are detected at one detector, we cannot figure out whether it was $|\Phi_{\mathrm{P}}^{+}\rangle$ or $|\Phi_{\mathrm{P}}^{-}\rangle$ which means a measurement failure. Thus, the success probability of the $\mathrm{B_P}$ measurement is also 1/2. We note that the success probability of any $\mathrm{B_P}$ measurement scheme using linear optical elements and photodetectors cannot be higher than 1/2 [24, 25].

All the deterministic Pauli operations for the polarized single-photon qubits are possible using half-wave plates [26]. The half-wave plate with fast axis $|F\rangle$ and slow axis $|S\rangle$ has the action

$$|F\rangle \rightarrow |F\rangle, \qquad |S\rangle \rightarrow -|S\rangle, \tag{2.26}$$

which induces a π phase shift in the slow axis. Suppose that the slow axis $|S\rangle$ makes an angle θ to the horizontal axis $|H\rangle$. The horizontally and vertically

polarized states after the action of the half-wave plate are

$$|H\rangle \rightarrow -\cos 2\theta|H\rangle - \sin 2\theta|V\rangle, \tag{2.27}$$

$$|V\rangle \rightarrow -\sin 2\theta|H\rangle + \cos 2\theta|V\rangle. \tag{2.28}$$

The Pauli X operation can be performed by applying the half-wave plate with $\theta = -\pi/4$, and the Pauli Z operation can be implemented by the half-wave plate with $\theta = \pi/2$.

2.3.3 Coherent-state qubits

The coherent states are generated by applying the displacement operator on the vacuum state. The displacement operator is defined as [27]

$$\hat{D}(\alpha) = \exp(\alpha\hat{a}^\dagger - \alpha^*\hat{a}), \tag{2.29}$$

where $\hat{a}$ ($\hat{a}^\dagger$) is the annihilation (creation) operator and α is an arbitrary complex number. The coherent state $|\alpha\rangle$ is then defined as a displaced vacuum state [28],

$$|\alpha\rangle = D(\alpha)|0\rangle. \tag{2.30}$$

Using the definition of the displacement operator, we can write the coherent state in the basis of Fock states $|n\rangle$:

$$|\alpha\rangle = e^{-|\alpha|^2/2} \sum_{n=0}^{\infty} \frac{\alpha^n}{\sqrt{n!}} |n\rangle, \tag{2.31}$$

and it can be shown that the coherent state $|\alpha\rangle$ is the eigenstate of the annihilation operation with its eigenvalue α,

$$\hat{a}|\alpha\rangle = \alpha|\alpha\rangle. \tag{2.32}$$

Another property of the coherent states is that they minimize the uncertainty relation with equally distributed uncertainties between two canonically conjugate quadrature operators:

$$\Delta q = \Delta p = 1/\sqrt{2}, \tag{2.33}$$

where $\hat{q} = (\hat{a} + \hat{a}^\dagger)/\sqrt{2}$ and $\hat{p} = (\hat{a} - \hat{a}^\dagger)/\sqrt{2}i$ are the quadrature operators, $\Delta q = \sqrt{\langle \hat{q}^2 \rangle - \langle \hat{q} \rangle^2}$ and $\Delta p = \sqrt{\langle \hat{p}^2 \rangle - \langle \hat{p} \rangle^2}$. The coherent states are usually thought as the most classical-like states of all the quantum states, because they have the same uncertainty with the vacuum state (actually the vacuum state $|0\rangle$ is just the coherent state with $\alpha = 0$).

A coherent-state qubit can be constructed using two coherent states with same amplitude and opposite phases as a qubit basis, $\{|\alpha\rangle, |-\alpha\rangle\}$. These two

coherent states are not orthogonal to each other but they can be regarded as asymptotically orthogonal in the limit of large amplitude $|\alpha| \gg 1$, because their overlap $\langle\alpha|-\alpha\rangle = e^{-2|\alpha|^2}$ decreases exponentially with $|\alpha|$. A coherent-state qubit in this basis is

$$|\psi_C\rangle = \mu|\alpha\rangle + \nu|-\alpha\rangle, \tag{2.34}$$

with the normalization condition,

$$|\mu|^2 + |\nu|^2 + (\mu\nu^* + \mu^*\nu)e^{-2|\alpha|^2} = 1. \tag{2.35}$$

Alternatively, it is possible to define an exactly orthogonal qubit basis in terms of equal superposition states of two coherent states with same amplitude and opposite phases, $|\alpha\rangle \pm |-\alpha\rangle$, where the normalization factors are omitted. The Bell states of coherent states are constructed using the logical qubit basis, $\{|\alpha\rangle, |-\alpha\rangle\}$, as

$$|\Phi_C^{\pm}\rangle = N_\alpha^{\pm}(|\alpha\rangle|\alpha\rangle \pm |-\alpha\rangle|-\alpha\rangle), \tag{2.36}$$

$$|\Psi_C^{\pm}\rangle = N_\alpha^{\pm}(|\alpha\rangle|-\alpha\rangle \pm |-\alpha\rangle|\alpha\rangle), \tag{2.37}$$

where $N_\alpha^{\pm} = 1/\sqrt{2 \pm 2e^{-4|\alpha|^2}}$. We note that the Bell states of coherent states

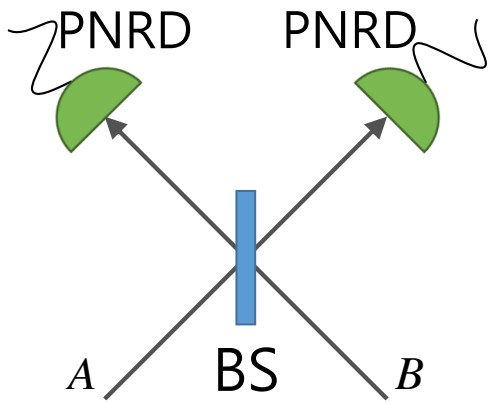

Figure 5: The Bell-state measurement for the coherent states, B_C, is implemented using a 50:50 beam splitter (BS) and two photon-number-resolving detectors (PNRD) [30].

are orthogonal to each other except the case of $|\Phi_C^+\rangle$ and $|\Psi_C^+\rangle$,

$$\langle\Phi_C^+|\Psi_C^+\rangle = \frac{1}{\cosh 2|\alpha|^2}, \tag{2.38}$$

which is because of the nonorthogonality of the logical qubit basis. It is reasonable to regard the Bell states of coherent states as asymptotically orthogonal, because the nonzero overlap of $|\Phi_C^+\rangle$ and $|\Psi_C^+\rangle$ rapidly decreases as $|\alpha|$ grows, and they are also called quasi-Bell states [29].

We consider the quantum teleportation of the coherent-state qubit $|\psi_C\rangle$ using one of the Bell states, $|\Psi_C^-\rangle$, as a channel state. The total product state

of the input state and the channel state can be written as

$$
\begin{aligned}
&|\psi_{\mathrm{C}}\rangle_A|\Psi_{\mathrm{C}}^-\rangle_{BC} \\
&= (\mu|\alpha\rangle_A + \nu|-\alpha\rangle_A)N_\alpha^-(|\alpha\rangle_B|-\alpha\rangle_C - |-\alpha\rangle_B|\alpha\rangle_C) \\
&= \frac{1}{2}\Bigg[-\frac{N_\alpha^-}{N_\alpha^+}|\Phi_{\mathrm{C}}^+\rangle_{AB}(\nu|\alpha\rangle_C - \mu|-\alpha\rangle_C) + |\Phi_{\mathrm{C}}^-\rangle_{AB}(\nu|\alpha\rangle_C + \mu|-\alpha\rangle_C) \\
&\quad - \frac{N_\alpha^-}{N_\alpha^+}|\Psi_{\mathrm{C}}^+\rangle_{AB}(\mu|\alpha\rangle_C - \nu|-\alpha\rangle_C) - |\Psi_{\mathrm{C}}^-\rangle_{AB}(\mu|\alpha\rangle_C + \nu|-\alpha\rangle_C)\Bigg]. \quad (2.39)
\end{aligned}
$$

The Bell-state measurement for the coherent states, $\mathrm{B_C}$, is implemented in a nearly deterministic way using a 50:50 beam splitter and two photon-number-resolving detectors as shown in Fig. 5 [30]. The photon-number-resolving detectors are required to perform number parity measurement which discriminates between even and odd numbers of photons. The operation of the beam splitter $U_{A,B}$ on coherent states is characterized as

$$U_{A,B}|\alpha\rangle_A|\beta\rangle_B = |(\alpha+\beta)/\sqrt{2}\rangle_A|(-\alpha+\beta)/\sqrt{2}\rangle_B. \quad (2.40)$$

The Bell states of coherent states after passing through the beam splitter $U_{A,B}$ are

$$|\Phi_{\mathrm{C}}^\pm\rangle_{AB} \xrightarrow{BS} N_\alpha^\pm(|\sqrt{2}\alpha\rangle \pm |-\sqrt{2}\alpha\rangle)_A|0\rangle_B, \quad (2.41)$$

$$|\Psi_{\mathrm{C}}^\pm\rangle_{AB} \xrightarrow{BS} N_\alpha^\pm|0\rangle_A(|\sqrt{2}\alpha\rangle \pm |-\sqrt{2}\alpha\rangle)_B, \quad (2.42)$$

where $|\mathrm{even}\rangle \equiv N_\alpha^+(|\sqrt{2}\alpha\rangle + |-\sqrt{2}\alpha\rangle)$ and $|\mathrm{odd}\rangle \equiv N_\alpha^-(|\sqrt{2}\alpha\rangle - |-\sqrt{2}\alpha\rangle)$

are even and odd number states which only contain even and odd numbers of photons, respectively, as

$$|\text{even}\rangle = 2N_{\alpha}^{+} e^{-|\alpha|^2} \sum_{n=0}^{\infty} \frac{(\sqrt{2}\alpha)^{2n}}{\sqrt{(2n)!}} |2n\rangle, \tag{2.43}$$

$$|\text{odd}\rangle = 2N_{\alpha}^{-} e^{-|\alpha|^2} \sum_{n=0}^{\infty} \frac{(\sqrt{2}\alpha)^{(2n+1)}}{\sqrt{(2n+1)!}} |2n+1\rangle. \tag{2.44}$$

The four Bell states of coherent states can be discriminated using two photon-number-resolving measurements as

$$\begin{aligned} &(\text{even},0) : \Phi_{\text{C}}^{+}, && (\text{odd},0) : \Phi_{\text{C}}^{-}, \\ &(0,\text{even}) : \Psi_{\text{C}}^{+}, && (0,\text{odd}) : \Psi_{\text{C}}^{-}. \end{aligned} \tag{2.45}$$

If even number of photons are detected at mode A and no photon is detected at mode B, it means that the Bell state was $|\Phi_{\text{C}}^{+}\rangle$, and so on. The failure of B_{C} occurs when both the detectors are silent due to the vacuum portion in state $|\text{even}\rangle$. In that case, we cannot distinguish whether the Bell state was $|\Phi_{\text{C}}^{+}\rangle$ or $|\Psi_{\text{C}}^{+}\rangle$, which is because of the nonzero overlap of these two Bell states. The failure probability of the B_{C} measurement for the case in Eq. (2.39) is given as

$$P_f = |{}_B\langle 0|_A\langle 0|U_{A,B}|\psi_{\text{C}}\rangle_A|\Psi_{\text{C}}^{-}\rangle_{BC}|^2 = \frac{e^{-2|\alpha|^2}}{1+e^{-2|\alpha|^2}}|\mu+\nu|^2, \tag{2.46}$$

which is negligible for sufficiently large $|\alpha|$ [31].

The Pauli X operation for the coherent-state qubits can be performed by a π phase shifter. However, the Pauli Z operation for the coherent-state qubits, which is nonunitary, can only be implemented probabilistically via quantum gate teleportation [19, 32]. Instead of probabilistic gate operation, there is a way to realize the Pauli Z operation approximately using the displacement operator [18]. By applying the displacement operator $\hat{D}(i\varepsilon)$ on the target state $|\psi_C\rangle = \mu|\alpha\rangle + \nu|-\alpha\rangle$, where ε is real, $\varepsilon^2 \ll 1$, and satisfies the relation $2\alpha\varepsilon = \frac{\pi}{2}$, we obtain the output state that the Pauli Z operation is accomplished approximately. The fidelity between the output state $\hat{D}(i\varepsilon)|\psi_C\rangle$ and the ideal state that the Pauli Z operation is performed perfectly, $\hat{Z}|\psi_C\rangle = \mu|\alpha\rangle - \nu|-\alpha\rangle$, is

$$\begin{aligned} |\langle\psi_C|\hat{Z}^\dagger\hat{D}(i\varepsilon)|\psi_C\rangle|^2 &= e^{-\varepsilon^2}||\mu|^2 + |\nu|^2 + ie^{-2\alpha^2}(\mu\nu^* - \mu^*\nu)|^2 \\ &\approx e^{-\varepsilon^2} \approx 1. \end{aligned} \tag{2.47}$$

Chapter 3

Transfer of different types of optical qubits over a lossy environment

We compare three different types of optical qubits for information transfer via quantum teleportation and direction transmission under photon losses. The three types of qubits are (1) qubits using the vacuum and the single-photon (VSP) states, (2) single-photon qubits using polarization degrees of freedom, i.e., polarized single-photon (PSP) qubits, and (3) coherent-state qubits that use two coherent states with opposite phases as the qubit basis. Our analysis shows that the teleportation scheme outperforms the direct transmission for most of cases as far as fidelities are concerned. Overall, VSP qubits are found to be the most efficient for both the direct transmission and teleportation under photon loss effects. The coherent-state qubits are more robust than PSP qubits either when their amplitudes are small as $|\alpha| \lesssim 1.22$ or when photon loss effects are strong. Our results would provide useful and timely information for the development of practical optical quantum information processing particularly in the context of hybrid architectures.

3.1 Introduction

Optical systems are one of the major candidates for implementations of quantum information processing. There are different ways for qubit encoding for optical quantum information processing. Probably, the most well-known method is to use a single photon with its polarization degree of freedom. Quantum teleportation experiments have been performed using such polarized single photons (PSPs) as qubits [13, 33] and quantum computing protocols based on linear optics have been developed along this line [14, 16]. It is also possible to use the vacuum and single-photon (VSP) states as the basis for qubit encoding [17, 23]. Coherent-state qubits have been studied as an alternative approach to optical quantum information processing [18, 19] with their advantages in teleportation [30, 34].

Efficient transfer of qubits is an important factor in quantum information processing. It is particularly crucial for quantum communication and quantum networks [35]. A comparison among the different types of qubits in terms of transfer efficiencies would be indispensable in order to build an efficient hybrid architecture for optical quantum information processing [36, 37, 38, 39, 40] in a lossy environment. There are different ways to transfer qubits, for example, such as direct transmission and quantum teleportation [9]. Takeoka *et al.* compared [41] the teleportation scheme for continuous-variable states [42, 43] with the direct transmission through a noisy channel. They showed that the teleportation scheme shows better transmission perfor-

mance than the direct transmission in strong decoherence regions [41]. Park and Jeong compared effects of photon losses and detection inefficiency on entangled coherent states and entangled photon-polarized states for quantum teleportation [44]. Extending these investigations, we are interested in comparisons for both the direct transmission and teleportation with the three aforementioned qubit-based approaches.

In this chapter, we investigate and compare fidelities of information transfer for the three different types of photonic qubits over a lossy environment. We find that teleportation is more robust to photon losses than the direct transmission for VSP qubits, PSP qubits, and coherent-state qubits with small amplitudes. While VSP qubits are the most robust ones to photon losses, coherent-state qubits with small amplitudes are more robust than the PSP qubits for optical quantum information transfer. In terms of the success probabilities for quantum teleportation based on linear optics, VSP qubits and coherent-state qubits are found to outperform PSP qubits under photon loss effects.

3.2 Direct transmission and teleportation for each type of qubits

3.2.1 Qubits using the vacuum and single-photon states

We first consider a VSP qubit,

$$|\psi_V\rangle = \mu|0\rangle + \nu|1\rangle, \tag{3.1}$$

where $|0\rangle$ and $|1\rangle$ are the vacuum and single-photon states, respectively. This type of encoding strategy is sometimes referred to as the single-rail logic because it is defined by the occupation of a single optical mode [17, 23]. State preperations and operations have been demonstrated experimentally using the single-rail logic [45, 46, 47, 48]. The time evolution of density operator ρ under photon losses is governed by the Born-Markov master equation [49],

$$\frac{\partial\rho}{\partial\tau} = \hat{J}\rho + \hat{L}\rho, \tag{3.2}$$

where τ is the interaction time,

$$\hat{J}\rho = \gamma\Sigma_i a_i \rho a_i^\dagger, \tag{3.3}$$

$$\hat{L}\rho = -(\gamma/2)\Sigma_i (a_i^\dagger a_i \rho + \rho a_i^\dagger a_i), \tag{3.4}$$

and γ is the decay constant. The general solution of Eq. (3.2) is written as,

$$\rho(\tau) = \exp[(\hat{J}+\hat{L})\tau]\rho(0), \tag{3.5}$$

where $\rho(0)$ is the initial density operator [50]. A VSP qubit under the direct transmission with photon losses is simply obtained as

$$\rho_{\mathrm{V}}^{D}(\tau) = (|\mu|^2 + |\nu|^2 r^2)|0\rangle\langle 0| + |\nu|^2 t^2 |1\rangle\langle 1| + t(\mu\nu^*|0\rangle\langle 1| + \mu^*\nu|1\rangle\langle 0|), \tag{3.6}$$

where $\mu = \cos(\theta/2)$, $\nu = e^{i\phi}\sin(\theta/2)$, $t = e^{-\gamma\tau/2}$, and $r = \sqrt{1-e^{-\gamma\tau}}$. The average fidelity between input and output states is

$$F_{\mathrm{V}}^{D}(\tau) = \frac{1}{4\pi}\int_0^{2\pi}\int_0^{\pi}\langle\psi_{\mathrm{V}}|\rho_{\mathrm{V}}^{D}(\tau)|\psi_{\mathrm{V}}\rangle \sin\theta \mathrm{d}\theta\mathrm{d}\phi = \frac{1}{2} + \frac{t}{3} + \frac{t^2}{6}. \tag{3.7}$$

A schematic comparison between the direct transmission and the teleportation process is presented in Fig. 6. In general, the quantum teleporation protocol for a qubit [9] requires a bipartite entangled state as the quantum channel in addition to a Bell-state measurement scheme that discriminates the four entangled states called the Bell states. The sender's outcome for the Bell-state measurement is sent to the receiver through a classical channel so that the input state can be reconstructed by the receiver using an appropriate unitary transform (U in Fig. 6) [9].

We now consider quantum teleportation of the VSP qubit using an en-

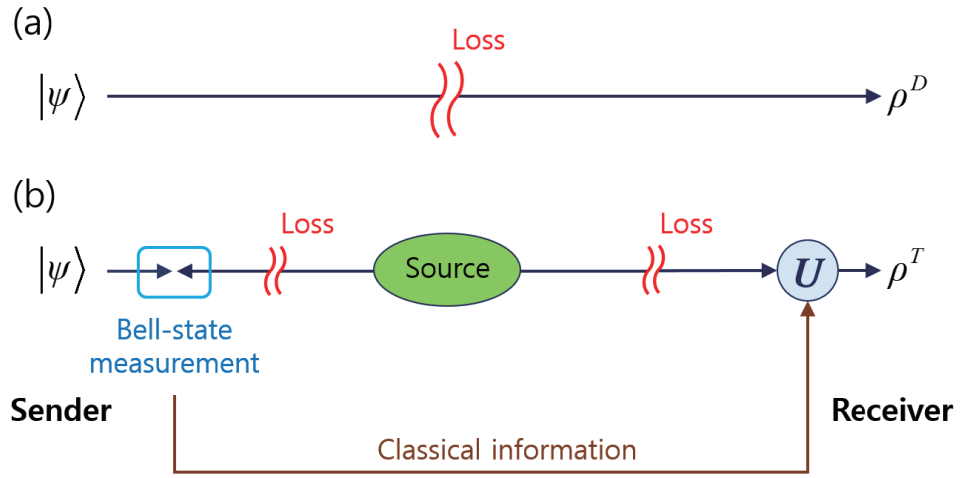

Figure 6: Schematics of two different ways to transfer qubits, i.e., (a) direct transmission and (b) quantum teleportation. The state $|\psi\rangle$ represents the unknown input state, and ρ^D and ρ^T represent the transfered states by means of each information transfer scheme, respectively.

tangled channel: $|\Psi_V^-\rangle = (|01\rangle - |10\rangle)/\sqrt{2}$, where $|01\rangle = |0\rangle \otimes |1\rangle$, etc. The entangled channel at time τ is obtained using Eq. (3.2) as

$$\rho_V^{ch}(\tau) = t^2 |\Psi_V^-\rangle\langle\Psi_V^-| + r^2 |00\rangle\langle 00|, \tag{3.8}$$

with which the teleportation is performed. The interaction time here should be half of the interaction time for the direct transmission because each part of entangled channel travels half of the length for the direct transmission as depicted in Fig. 6. The Bell-state measurement is performed to discriminate between the four Bell states, $|\Phi_V^{\pm}\rangle$ and $|\Psi_V^{\pm}\rangle$ defined in Eqs. (2.14) and (2.15), as a joint measurement for the input state and the sender's part of the entangled

channel. If the outcome of the Bell-state measurement was $|\Psi_{\rm V}^{+}\rangle$, the required unitary transform is the σ_z operation that corresponds to π phase shift. If the outcome was $|\Psi_{\rm V}^{-}\rangle$, the receiver does not need to do anything. However, a typical Bell measurement scheme using linear optics and photodetectors [23] cannot discriminate the other two Bell state, $|\Phi_{\rm V}^{\pm}\rangle$, so that the success probability is limited to 50% [23, 51]. The teleported state after an appropriate unitary transform is

$$\rho_{\rm V}^{T}(\tau) = \left(\frac{t^2}{4} + \frac{|\nu|^2 r^2}{2}\right)^{-1} \left(\frac{t^2}{4}|\psi_{\rm V}\rangle\langle\psi_{\rm V}| + \frac{|\nu|^2 r^2}{2}|0\rangle\langle 0|\right), \tag{3.9}$$

and the average success probability is

$$\begin{aligned} P_{\rm V} = {\rm Tr}\left[\langle\Psi_{\rm V}^{+}|\left\{|\psi_{\rm V}\rangle\langle\psi_{\rm V}| \otimes \rho_{\rm V}^{ch}(\tau/2)\right\}|\Psi_{\rm V}^{+}\rangle\right]_{\rm avg} \\ + {\rm Tr}\left[\langle\Psi_{\rm V}^{-}|\left\{|\psi_{\rm V}\rangle\langle\psi_{\rm V}| \otimes \rho_{\rm V}^{ch}(\tau/2)\right\}|\Psi_{\rm V}^{-}\rangle\right]_{\rm avg} = 1/2, \end{aligned} \tag{3.10}$$

where average is taken over the Bloch sphere of the input state. Interestingly, the success probability is not affected by photon losses even though the average fidelity is degraded as already implied in Eq. (3.9). The average fidelity for the successful events obtained in the same way as the case of the direct transmission is

$$F_{\rm V}^{T}(\tau/2) = \frac{1}{2(1-t)} + \frac{t^2}{4(1-t)^2}\log\frac{t}{2-t}, \tag{3.11}$$

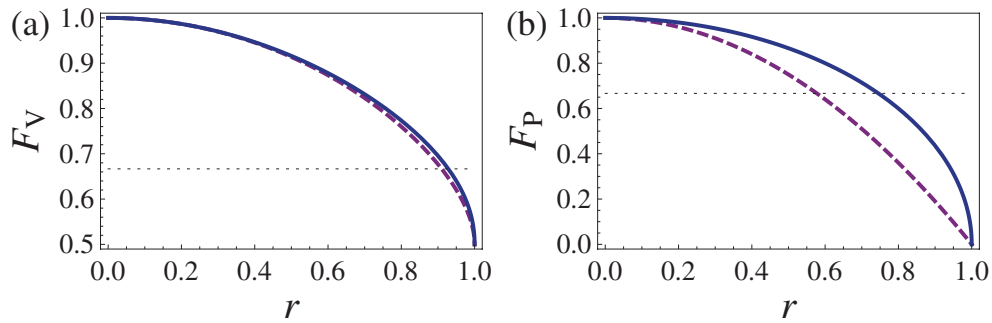

Figure 7: Average fidelities of teleportation and direct transmission for (a) VSP qubits ($F_{\rm V}$) and (b) PSP qubits ($F_{\rm P}$) against the normalized time r. The solid curves represent the average fidelities for teleportation and the dashed curves correspond to those of the direct transmission. The horizontal dotted line indicates classical limit, $2/3$, which can be achieved by using a separable teleportation channel.

where τ was replaced by $\tau/2$ for a comparison with the direct transmission. As shown in Fig. 7(a), the average fidelity of teleportation $F_{\rm V}^T$ is always higher than that of the direct transmission $F_{\rm V}^D$. The figure also shows that $F_{\rm V}^T$ goes below the classical limit 2/3 [21] at $r \simeq 0.928$ while $F_{\rm V}^D$ does so at $r \simeq 0.910$.

3.2.2 Polarized single-photon qubits

A PSP qubit is represented as

$$|\psi_{\rm P}\rangle = \mu|H\rangle + \nu|V\rangle, \tag{3.12}$$

where $|H\rangle$ and $|V\rangle$ correspond to horizontally and vertically polarized states, respectively. Using Eq. (3.2), it is straightforward to find that a PSP qubit in

the direct transmission under photon losses evolves as

$$\rho_{\mathrm{P}}(\tau) = t^2 |\psi_{\mathrm{P}}\rangle\langle\psi_{\mathrm{P}}| + r^2 |0\rangle\langle 0| \tag{3.13}$$

and the average fidelity is obtained as $F_{\mathrm{P}}^{D}(\tau) = t^2$. We then consider quantum teleportation for a PSP qubit using an entangled channel: $|\Psi_{\mathrm{P}}^{-}\rangle = (|HV\rangle - |VH\rangle)/\sqrt{2}$. The entangled channel at time τ obtained using Eq. (3.2) is

$$\rho_{\mathrm{P}}^{ch}(\tau) = t^4 |\Psi_{\mathrm{P}}^{-}\rangle\langle\Psi_{\mathrm{P}}^{-}| + 2r^2 t^2 \tilde{\rho} + r^4 |00\rangle\langle 00|, \tag{3.14}$$

where

$$\tilde{\rho} = \left(|H0\rangle\langle H0| + |V0\rangle\langle V0| + |0H\rangle\langle 0H| + |0V\rangle\langle 0V|\right)/4. \tag{3.15}$$

Here, the four Bell states are $|\Phi_{\mathrm{P}}^{\pm}\rangle$ and $|\Psi_{\mathrm{P}}^{\pm}\rangle$ defined in Eqs. (2.21) and (2.22). The Bell-state measurement can be performed using a 50:50 beam splitter, two polarizing beam splitters, and four photodetectors [24]. The teleported state after the Bell-state measurement and a correct unitary transform is found to be identical to $\rho_{\mathrm{P}}(\tau)$ for the case of the direct transmission in Eq. (3.13). Again, only two of the Bell states, $|\Psi_{\mathrm{P}}^{\pm}\rangle$, can be identified using linear optics [24, 25] and required unitary transforms are the identity operation and the σ_z operation that is realized with a half-wave plate. The average success

probability is

$$P_{\mathrm{P}} = \mathrm{Tr}\left[\langle\Psi_{\mathrm{P}}^{+}|\left\{|\psi_{\mathrm{P}}\rangle\langle\psi_{\mathrm{P}}|\otimes\rho_{\mathrm{P}}^{ch}(\tau/2)\right\}|\Psi_{\mathrm{P}}^{+}\rangle\right]_{\mathrm{avg}} + \mathrm{Tr}\left[\langle\Psi_{\mathrm{P}}^{-}|\left\{|\psi_{\mathrm{P}}\rangle\langle\psi_{\mathrm{P}}|\otimes\rho_{\mathrm{P}}^{ch}(\tau/2)\right\}|\Psi_{\mathrm{P}}^{-}\rangle\right]_{\mathrm{avg}} = t/2. \tag{3.16}$$

In fact, the success probability in this case is identical for any input state. It is worth noting that the success probability of PSP qubits is always lower than the success probability of VSP qubits. We obtain the average fidelity for the successful events as $F_{\mathrm{P}}^{T}(\tau/2) = t$, where $\tau/2$ replaces τ for a comparison with the direct transmission as mentioned in Sec. 3.2.1. We plot $F_{\mathrm{P}}^{D}(\tau) = t^2$ and $F_{\mathrm{P}}^{T}(\tau/2) = t$ in Fig. 7(b). Obviously, F_{P}^{T} is always higher than F_{P}^{D}, and F_{P}^{T} goes below the classical limit 2/3 at $r \simeq 0.745$ while F_{P}^{D} does so at $r \simeq 0.577$.

3.2.3 Coherent-state qubits

Instead of single photons, superpositions of coherent states can be used for quantum information processing with their inherent advantages. The small-size implementations of superpositions of coherent states have been performed [52, 53, 54, 55, 56, 57, 58] up to $\alpha \sim 1.6$ [54, 55, 58] and arbitrary qubits were demonstrated [59]. Their large-size implementation is possible using the non-deterministic amplification scheme [60, 61], a Fock state with a large number [54, 62, 63], or multiple photon subtractions [64, 65] but it is yet experimentally challenging.

Coherent-state qubits not only lose their coherence but also undergo am-

plitude damping under photon losses. However, as the interaction time τ is the value known to the sender and the receiver, we can use $|\pm t\alpha\rangle$ as a dynamic qubit basis in order to reflect the amplitude damping as suggested in Ref. [30]. Adopting damped coherent states $|\pm t\alpha\rangle$ as the dynamic qubit basis, the time-dependent target coherent-state qubit which we want the receiver to have is

$$|\psi_C(\tau)\rangle = N(\tau)\left(\mu|t\alpha\rangle + \nu|-t\alpha\rangle\right), \tag{3.17}$$

where μ, ν are some complex numbers and $N(\tau)$ is normalization constant. To achieve this purpose, the sender actually transmits the state $|\psi_C(\tau=0)\rangle$. It is straightforward to find that the initial state $|\psi_C(\tau=0)\rangle$ under direct transmission evolves to

$$\begin{aligned}\rho_C^D(\tau) = |N(\tau=0)|^2\Big\{ & |\mu|^2|t\alpha\rangle\langle t\alpha| + |\nu|^2|-t\alpha\rangle\langle -t\alpha| \\ & + e^{-2|\alpha|^2 r^2}(\mu\nu^*|t\alpha\rangle\langle -t\alpha| + \mu^*\nu|-t\alpha\rangle\langle t\alpha|)\Big\}.\end{aligned} \tag{3.18}$$

Since the coherent states $|\pm t\alpha\rangle$ are not orthogonal to each other, we need an orthonormal basis which spans the input and the output states in order to obtain average fidelity on the Bloch sphere. We take such a basis, $|\pm(t)\rangle \propto |t\alpha\rangle \pm |-t\alpha\rangle$, where the normalization factors are omitted. The input state is

then represented as

$$|\psi_{\rm C}(\tau)\rangle = \cos(\theta/2)|+(t)\rangle + \sin(\theta/2)e^{i\phi}|-(t)\rangle, \tag{3.19}$$

so that the average can be taken over θ and ϕ. The average fidelity between $|\psi_{\rm C}(\tau)\rangle$ and $\rho_{\rm C}^{D}(\tau)$ is obtained as

$$F_{\rm C}^{D}(\tau) = \frac{1}{6\left(e^{4|\alpha|^2}-1\right)}\Big\{-3(1-e^{4|\alpha|^2}) - e^{2|\alpha|^2 r^2}(1-e^{4|\alpha|^2 t^2}) + \left(e^{4|\alpha|^2} + e^{2|\alpha|^2(2-r^2)}\right)\sqrt{1-e^{-4|\alpha|^2}}\sqrt{1-e^{-4|\alpha|^2 t^2}}\Big\}. \tag{3.20}$$

The average fidelity of teleportation was derived in Ref. [44] using the methods described in the previous subsections. To perform teleportation for a coherent-state qubit, an entangled coherent state $|\Psi_{\rm C}^{-}\rangle = N_{\alpha}^{-}(|\alpha\rangle|-\alpha\rangle - |-\alpha\rangle|\alpha\rangle)$ is shared by the sender and the receiver. The Bell-state measurement are supposed to discriminate between the states,

$$|\Phi_{\rm C}^{\pm}(\tau)\rangle = N_{\alpha}^{\pm}(\tau)(|t\alpha\rangle|t\alpha\rangle \pm |-t\alpha\rangle|-t\alpha\rangle), \tag{3.21}$$

$$|\Psi_{\rm C}^{\pm}(\tau)\rangle = N_{\alpha}^{\pm}(\tau)(|t\alpha\rangle|-t\alpha\rangle \pm |-t\alpha\rangle|t\alpha\rangle), \tag{3.22}$$

where $N_{\alpha}^{\pm}(\tau) = 1/\sqrt{2\pm 2e^{-4t^2|\alpha|^2}}$. This type of Bell-state measurement can be performed using a 50:50 beam splitter and two photon-number-resolving detectors [30]. The two measurement outcomes, $|\Psi_{\rm C}^{-}(\tau)\rangle$ and $|\Phi_{\rm C}^{-}(\tau)\rangle$, require straightforward unitary transforms (identity and π phase shift) and we take

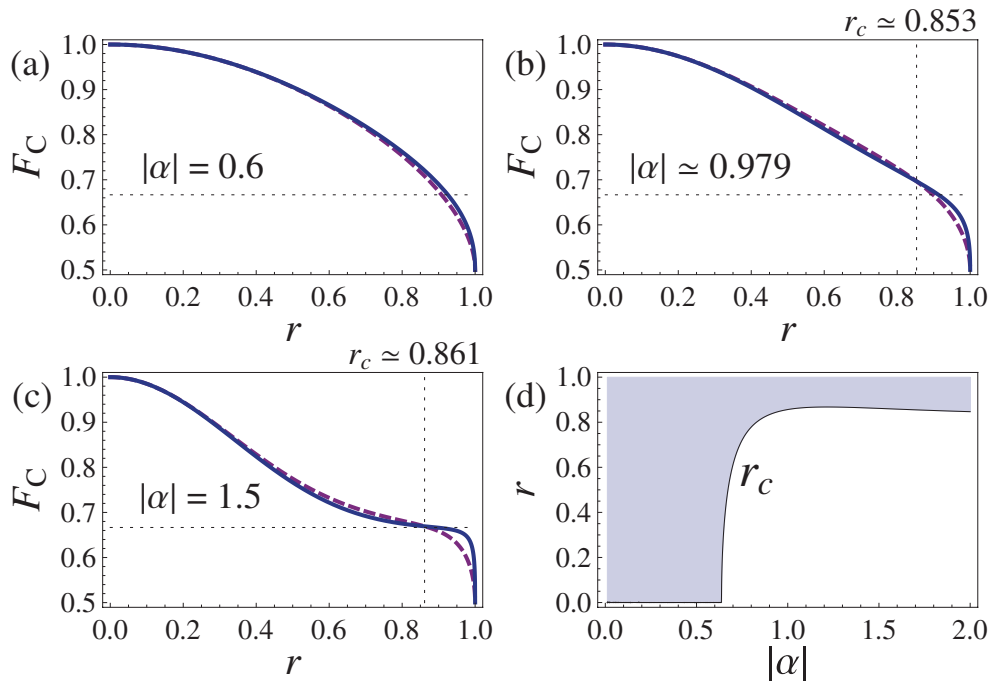

Figure 8: (a)-(c) Average fidelities F_C of teleportation (solid curve) and direct transmission (dashed curve) for coherent-state qubits with amplitudes (a) $|\alpha| = 0.6$, (b) $|\alpha| \simeq 0.979$ and (c) $|\alpha| = 1.5$ against the normalized time r. The horizontal dotted lines indicate the classical limit, 2/3. (d) The shaded area indicates the region where the teleportation outperforms the direct transmission. The time boundary between the teleportation-efficient and direct-transmission-efficient regions is indicated by r_c.

them as the successful events following Ref. [44].

By substituting τ in Ref. [44] with $\tau/2$ for a comparison with direct transmission as mentioned in Secs. 3.2.1 and 3.2.2, the average fidelity of telepor-

tation for the successful events is

$$F_{\mathrm{C}}^{T}(\tau/2) = \frac{1}{2}\mathrm{csch}\,A\,\Big\{\mathrm{csch}\,A\,\sinh^{2}\left(2|\alpha|^{2}t\right)\cosh\left(A-2|\alpha|^{2}\right) \times \tanh^{-1}\left(\mathrm{csch}2|\alpha|^{2}\sinh A\right) - \sinh 2|\alpha|^{2}\cosh\left(2|\alpha|^{2}t\right)\Big\}, \quad (3.23)$$

where $A = 2|\alpha|^{2}(t-1)$. The average success probability was shown to be $P_{\mathrm{C}} = 1/2$ [44]. This is identical to that of VSP qubits, which is always higher than that of PSP qubits. We plot $F_{\mathrm{C}}^{D}(\tau)$ and $F_{\mathrm{C}}^{T}(\tau/2)$ for several amplitudes of $|\alpha|$'s in Figs. 8(a)-8(c). If the amplitudes of coherent-state qubits are as small as $|\alpha| \lesssim 0.636$, F_{C}^{T} is always higher than F_{C}^{D}. However, as $|\alpha|$ gets larger, the region where teleportation outperforms diminishes. The direct transmission outperforms for the weaker decoherence $r < r_{c}$, whereas the teleportation is better for the stronger decoherence $r > r_{c}$ [Fig. 8(d)].

3.3 Comparing different types of qubits

We now compare VSP qubits, PSP qubits, and coherent-state qubits under each information transfer scheme. The average fidelities for direct transmission and teleportation of VSP, PSP, and coherent-state qubits with $0 \leq |\alpha| \leq 3$ are plotted in Figs. 9(a) and 9(b). In both the schemes, VSP qubits are the most robust ones to decoherence in the region where comparing fidelities is meaningful, i.e., above the classical bound $2/3$. Using direct transmission (teleportation), the coherent-state qubits with small $|\alpha| \lesssim 1.222$ ($|\alpha| \lesssim 0.802$ for the

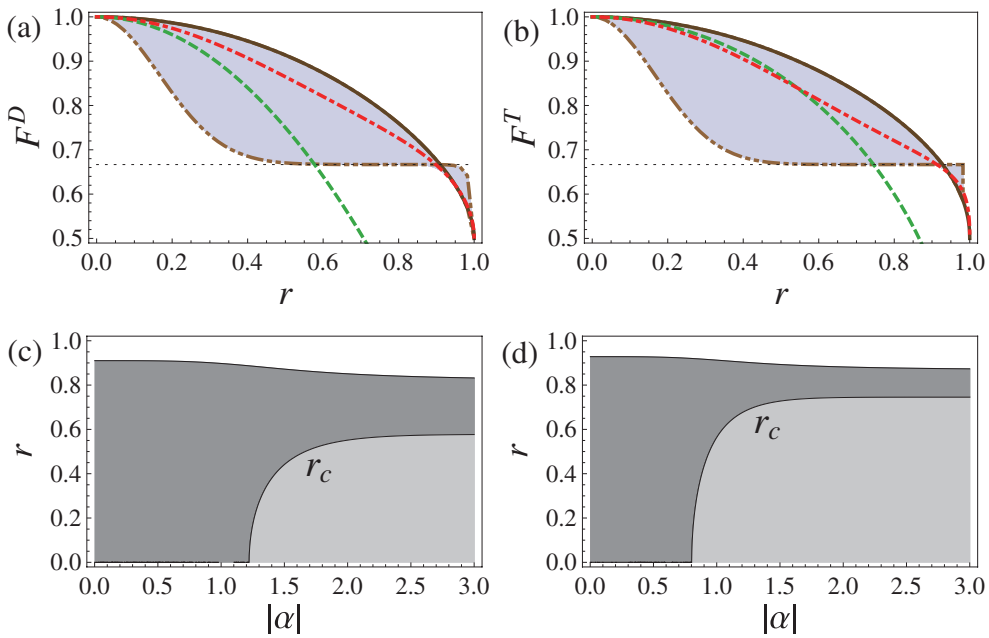

Figure 9: The upper figures show the average fidelities for (a) direct transmission and (b) quantum teleportation against the normalized time r. The solid and dashed curves represent the VSP and PSP qubits, respectively. The dot-dashed curve corresponds to the coherent-state qubits with $|\alpha| \simeq 0.979$, and the double-dot-dashed curve to the coherent-state qubits with $|\alpha| = 3$. The shaded area is for the coherent-state qubits with $0 \leq |\alpha| \leq 3$. The lower figures compare PSP and coherent-states qubits. The coherent-state qubits outperform PSP qubits in the dark-shaded regions while PSP qubits work better in the light-shaded regions for (c) direct transmission and (d) teleportation. In the unshaded regions of panels (c) and (d), both the fidelities are smaller than the classical bound $2/3$.

teleportation case) outperforms PSP qubits in the entire region of r where the comparison is valid. However, as $|\alpha|$ gets larger, the regions where coherent-state qubits outperforms PSP qubits diminish. Coherent-state qubits outperform PSP qubits for the stronger decoherence $r > r_c$, whereas PSP qubits outperform coherent-state qubits for the weaker decoherence $r < r_c$ [Figs. 9(c) and 9(d)].

Considering the number of photons as a resource, we may compare PSP qubits and coherent-state qubits when they have the same average photon number, i.e., $\langle \hat{n} \rangle_{\rm avg} = 1$. The average photon number of input coherent-state qubits $|\psi_{\rm C}(\tau = 0)\rangle$ is

$$\langle \hat{n} \rangle_{\rm avg} = \frac{1}{4\pi} \int_0^{2\pi} \int_0^{\pi} \langle \psi_{\rm C}(0)|\hat{n}|\psi_{\rm C}(0)\rangle \sin\theta d\theta d\phi = \frac{|\alpha|^2}{\tanh(2|\alpha|^2)}, \qquad (3.24)$$

where $\hat{n} = a^\dagger a$. Therefore, the amplitude of coherent-state qubits for a comparison should be $|\alpha| \simeq 0.979$ for $\langle \hat{n} \rangle_{\rm avg} = 1$ to be the same to that of the PSP qubits. The coherent-state qubits with the chosen amplitude $|\alpha| \simeq 0.979$ always outperform PSP qubits when the direct transmission is used as shown in Fig. 9(a). However, when the teleportation protocol is used, PSP qubits are more robust than coherent-state qubits with the chosen amplitude when decoherence is weak, and the opposite is true for strong decoherence [Fig. 9(b)]. The PSP qubits in both schemes eventually become the vacuum states, which leads their fidelities in Fig. 9 to vanish as $r \to 1$.

The coherent-state qubits and the VSP qubits become identical in the

limit of $\alpha \to 0$ as implied in Figs. 9(a) and 9(b). This is due to the fact that even and odd superpositions of coherent sates, $|\alpha\rangle \pm |-\alpha\rangle$ (without normalization), approach the vacuum and single photon, respectively [66].

3.4 Remarks

Several different types of qubits have been suggested for optical quantum information processing and each of them has its own merits and limitations. A hybrid architecture using different types of qubits may be an efficient way to implement practical quantum information processing based on optical systems [36, 37, 38]. In this context, it is important to make a thorough comparison among the different types of qubits in terms of transfer efficiencies in a lossy environment. We have compared three well-known different types of optical qubits, VSP, PSP and coherent-state qubits, for information transfer via quantum teleportation and direction transmission under photon losses.

Of course, it should be noted that quantum teleportation always suffers lower success probabilities compared to the direct transmission if available resources are limited to linear optics elements and photon detectors in addition to the entangled pair [24, 25]. However, as far as fidelities are concerned, quantum teleportation always outperforms the direct transmission when VSP and PSP qubits are used. The same applies to the coherent-state qubits when their amplitudes are as small as $|\alpha| \lesssim 0.636$. On the other hand, the teleportation outperforms the direct transmission in the strong decoherence regions

for the coherent-state qubits with large amplitudes.

We have found that VSP qubits are the most robust ones against photon losses both for quantum teleportation and for the direct transmission. Coherent-state qubits with small amplitudes ($|\alpha| \lesssim 1.222$ for direct transmission and $|\alpha| \lesssim 0.802$ for teleportation) are more robust to photon losses than PSP qubits in optical quantum information transfer, whereas the coherent-state qubits with large amplitudes outperform PSP qubits only in the strong decoherence regions. This means that coherent-state qubits may be more effective than PSP qubits for optical quantum information transfer particularly when photon loss effects are heavy. The success probabilities for teleportation of coherent-state qubits and VSP qubits (i.e., 1/2 regardless of losses) are always greater than that of PSP qubits (i.e., smaller than 1/2 under lossy effects). Overall, VSP qubits are the most efficient for quantum information transfer under photon loss effects among the three types of qubits.

In spite of our results, clearly unfavorable to the PSP qubits, the PSP qubits may be preferred for certain applications such as quantum key distribution using single photons in which post-selection plays an important role [67]. In this type of post-selection process, a result is simply discarded whenever any photon is missing at the final measurement. This is not so straightforward with the VSP or coherent-state qubits because the photon numbers of those qubits are inherently indefinite.

In this chapter, we have compared three types of optical qubits that can be represented by single-mode states. Our results would provide useful and

timely information for the development of practical optical quantum information processing. It would be an interesting future work to extend this comparison to optical qudits [68, 69], continuous variable systems [70], and hybrid qubits [38, 39, 40].

Chapter 4

Two different types of optical hybrid qubits for teleportation in a lossy environment

We investigate the performance of quantum teleportation under a lossy environment using two different types of optical hybrid qubits. One is the hybrid of a polarized single-photon qubit and a coherent-state qubit (type-I logical qubit), and the other is the hybrid of a qubit of the vacuum and the single-photon and a coherent-state qubit (type-II logical qubit). We show that type-II hybrid qubits are generally more robust to photon loss effects compared to type-I hybrid qubits with respect to fidelities and success probabilities of quantum teleportation.

4.1 Introduction

Quantum teleportation is a protocol to transfer an unknown qubit from one place to another via an entangled quantum channel [9, 13, 71]. It is at the heart of various applications in quantum communication and computation. In particular, it plays a crucial role in implementing all-optical quantum computation [12, 15, 16, 32, 72, 73]. A typical qubit for optical quantum teleportation utilizes the horizontal and vertical polarization states of a single

photon, $\{|H\rangle, |V\rangle\}$ [13, 16, 72, 73], or alternatively the vacuum and single-photon states, $\{|0\rangle, |1\rangle\}$ [17, 23]. However, in this type of approaches based on a single-photon qubit, the success probability of a Bell-state measurement, which is an essential element in realizing the quantum teleportation protocol, cannot exceed 1/2 using linear optics and photon detection [24, 25]. Efforts are being made to overcome this limitation using auxiliary states, additional operations or multipartite encoding [74, 75, 76, 77, 78], while each of them has its own price to pay. An alternative approach employs coherent states as the qubit basis, $\{|\alpha\rangle, |-\alpha\rangle\}$ [30, 34], where $\pm\alpha$ are amplitudes of the coherent states. It enables one to implement a nearly deterministic Bell-state measurement [18, 19, 29, 30]. However, due to the non-orthogonality of two coherent states, $|\alpha\rangle$ and $|-\alpha\rangle$, a necessary operation to finish the teleportation process such as the Pauli-Z operation cannot be performed in a deterministic way and produces additional errors [15, 32].

Recently, a hybrid approach to optical quantum information processing was proposed by combining advantages of the two aforementioned approaches [38]. In this approach, the logical qubit is constructed using entanglement between the polarization states of a single photon and coherent states that leads to nearly deterministic quantum controls [38]. It enables one to perform a near-deterministic quantum teleportation as well as near-deterministic universal gate operations in a more efficient manner compared to previous approaches [12, 15, 16, 32, 72, 73]. The required resource is hybrid states in the form of $|\mathrm{H_I}\rangle = |H\rangle|\alpha\rangle + |V\rangle|-\alpha\rangle$ [38]. Within this context, it was shown that

such a hybrid entanglement is useful for teleportation between a polarized single-photon qubit and a coherent-state qubit [37] and for a loophole-free Bell inequality test [79]. However, it is known that the generation of entanglement between a polarized single photon and coherent states such as $|\mathrm{H_I}\rangle$ is highly demanding [80, 81, 82, 83]. There exists a recent theoretical proposal that enables one to efficiently generate the state $|\mathrm{H_I}\rangle$ based on parametric downconversion, linear optics elements, and photodetectors [84], while it requires preparation of a coherent-state superposition [54] as a resource.

On the other hand, the hybrid entanglement of the vacuum and the single photon (instead of single-photon polarization) with coherent states, such as $|\mathrm{H_{II}}\rangle = |0\rangle|\alpha\rangle + |1\rangle|-\alpha\rangle$, was successfully demonstrated in recent experiments [39, 40]. While $|\mathrm{H_{II}}\rangle$ is easier to generate than $|\mathrm{H_I}\rangle$, universal gate operations for a logical qubit in the form of $|\mathrm{H_{II}}\rangle$ are not so straightforward to implement. This is because single-qubit operations in the basis of the vacuum $|0\rangle$ and the single photon $|1\rangle$ except the phase rotation are basically nondeterministic [17]. Nevertheless, we have shown that the qubits utilizing the vacuum and the single photon basis are more robust against losses compared to the polarized single-photon qubits in Chap. 3.

Thus, the two types of hybrid states $|\mathrm{H_I}\rangle$ and $|\mathrm{H_{II}}\rangle$ have their own advantages and disadvantages compared to each other for quantum information processing. However, we still do not have any clear references about the choice of the type in a specific scenario of the implementation of quantum information protocols. Therefore, it may be essential to investigate two dis-

tinct approaches under the same circumstances, one based on the form of $|H_I\rangle$ and the other of $|H_{II}\rangle$, and compare their performances regarding noises or resources for quantum information processing.

In this chapter, we investigate the implementations of quantum teleportation in a lossy environment as a paradigmatic example to compare the two different types of hybrid qubits in the form of $|H_I\rangle$ and $|H_{II}\rangle$. We will consider the photon loss effect, which is the dominant noise factor for optical quantum information processing [15] among all possible decoherence effects during teleportation process [85, 86, 87]. We first analyze the effects of photon losses on the entangled quantum channel distributed between two separated parties, based on the two different hybrid states. We then compare their performances of quantum teleportation with respect to the average fidelity and the average success probability of teleportation. Our analysis shows that the quantum teleportation with the hybrid of a qubit of the vacuum and the single-photon and a coherent-state qubit $|H_{II}\rangle$ is more robust to photon losses than the hybrid of a polarized single-photon qubit and a coherent-state qubit $|H_I\rangle$.

4.2 Qunatum teleportation using hybrid qubits

4.2.1 Two types of optical hybrid qubits

Since there are a number of studies on quantum information processing using various kinds of optical hybrid systems [38, 39, 40, 88, 89, 90, 91, 92, 93, 94, 95, 96, 97, 98], we first need to clarify the types of optical hybrid qubits that

we consider in this chapter. The first one is the hybrid of a polarized single-photon qubit and a coherent-state qubit, which was originally used to propose the hybrid scheme of optical quantum information processing recently [38]. The other is the hybrid of a qubit of the vacuum and the single-photon and a coherent-state qubit, which was recently generated by experiments [39, 40]. We consider optical hybrid qubits constructed in the logical basis,

$$\{|0_L\rangle = |+\rangle|\alpha\rangle, |1_L\rangle = |-\rangle|-\alpha\rangle\}, \tag{4.1}$$

and the two different types of hybrid qubits are then defined as

I. the hybrid of a polarized single-photon qubit and a coherent-state qubit where $|\pm\rangle = (|H\rangle \pm |V\rangle)/\sqrt{2}$,

II. the hybrid of a qubit of the vacuum and the single-photon and a coherent-state qubit where $|\pm\rangle = (|0\rangle \pm |1\rangle)/\sqrt{2}$.

We will refer to the former as *type-I* hybrid qubit which is the same form used in Ref. [38], while the latter will be referred to as *type-II* hybrid qubit hereafter.

4.2.2 Teleportation scheme for hybrid qubits

In the standard quantum teleportation procedure [9], Alice is supposed to teleport an arbitrary unknown state,

$$|\phi\rangle = \mu|0_L\rangle + \nu|1_L\rangle, \tag{4.2}$$

to Bob via a maximally entangled quantum channel,

$$|\Psi_{ch}\rangle = (|0_L\rangle|0_L\rangle + |1_L\rangle|1_L\rangle)/\sqrt{2}. \tag{4.3}$$

Alice performs a Bell-state measurement on the unknown qubit and her part of the entangled channel and sends the measurement outcome to Bob. Bob applies an appropriate unitary transform on his state depending on Alice's measurement outcome in order to reconstruct the original qubit.

The hybrid teleportation scheme of type-I qubits is described in Ref. [38]. As shown in Fig. 10, Alice and Bob share a hybrid entangled channel in order to teleport a type-I hybrid qubit from Alice to Bob. The total product state of the unknown input state $|\phi\rangle$ and the channel state $|\Psi_{ch}\rangle$ in terms of the type-I hybrid encoding can be expressed as

$$\begin{aligned}|\phi\rangle_{aA}|\Psi_{ch}\rangle_{bBcC} = \frac{1}{2}\Big(&|\Phi_L^+\rangle_{aAbB}|\phi\rangle_{cC} + |\Phi_L^-\rangle_{aAbB}\hat{Z}|\phi\rangle_{cC} \\ &+ |\Psi_L^+\rangle_{aAbB}\hat{X}|\phi\rangle_{cC} + |\Psi_L^-\rangle_{aAbB}\hat{X}\hat{Z}|\phi\rangle_{cC}\Big),\end{aligned} \tag{4.4}$$

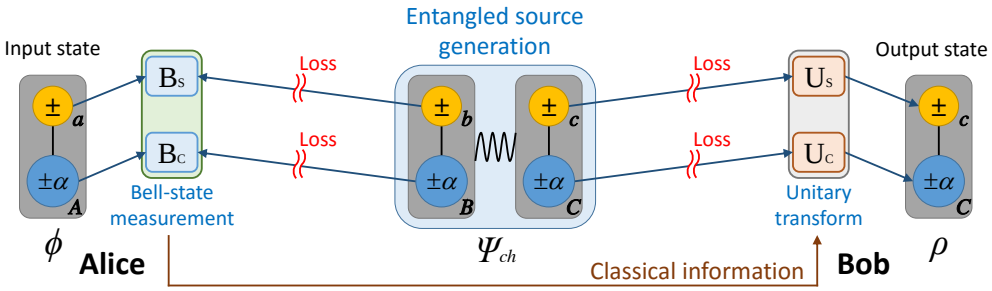

Figure 10: Schematic of hybrid quantum teleportation. Photon losses are supposed to occur in the channel state Ψ_{ch}. U_S (U_C) represents a unitary transform applied to a single-photon state (coherent state). ϕ and ρ represent the initial state and the final teleported state, respectively. The logical Bell-state measurement is composed of two elements, B_S and B_C, that correspond to Bell-state measurements for single-photon states and coherent states, respectively.

with logical Bell states

$$|\Phi_L^{\pm}\rangle = \frac{1}{\sqrt{2}}(|0_L\rangle|0_L\rangle \pm |1_L\rangle|1_L\rangle), \tag{4.5}$$

$$|\Psi_L^{\pm}\rangle = \frac{1}{\sqrt{2}}(|0_L\rangle|1_L\rangle \pm |1_L\rangle|0_L\rangle), \tag{4.6}$$

and Pauli operators $\hat{X}$ and $\hat{Z}$ in terms of the logical qubit basis, where subscripts a, b and c in Eq. (4.4) represent single-photon modes and A, B and C represent coherent-state modes as depicted in Fig. 10. This equation can be

rewritten as

$$
\begin{aligned}
|\phi\rangle_{aA}|\Psi_{ch}\rangle_{bBcC} =& \frac{1}{4}\Bigg[\left(\frac{|\Phi_{\rm P}^{+}\rangle_{ab}|\Phi_{\rm C}^{+}\rangle_{AB}}{N_{\alpha}^{+}} + \frac{|\Psi_{\rm P}^{+}\rangle_{ab}|\Phi_{\rm C}^{-}\rangle_{AB}}{N_{\alpha}^{-}}\right)|\phi\rangle_{cC} \\
&+ \left(\frac{|\Phi_{\rm P}^{+}\rangle_{ab}|\Phi_{\rm C}^{-}\rangle_{AB}}{N_{\alpha}^{-}} + \frac{|\Psi_{\rm P}^{+}\rangle_{ab}|\Phi_{\rm C}^{+}\rangle_{AB}}{N_{\alpha}^{+}}\right)\hat{Z}|\phi\rangle_{cC} \\
&+ \left(\frac{|\Phi_{\rm P}^{-}\rangle_{ab}|\Psi_{\rm C}^{+}\rangle_{AB}}{N_{\alpha}^{+}} - \frac{|\Psi_{\rm P}^{-}\rangle_{ab}|\Psi_{\rm C}^{-}\rangle_{AB}}{N_{\alpha}^{-}}\right)\hat{X}|\phi\rangle_{cC} \\
&+ \left(\frac{|\Phi_{\rm P}^{-}\rangle_{ab}|\Psi_{\rm C}^{-}\rangle_{AB}}{N_{\alpha}^{-}} - \frac{|\Psi_{\rm P}^{-}\rangle_{ab}|\Psi_{\rm C}^{+}\rangle_{AB}}{N_{\alpha}^{+}}\right)\hat{X}\hat{Z}|\phi\rangle_{cC}\Bigg], \quad (4.7)
\end{aligned}
$$

where $|\Phi_{\rm P}^{\pm}\rangle$ and $|\Psi_{\rm P}^{\pm}\rangle$ are the Bell states of polarized single-photon states defined in Eqs. (2.21) and (2.22), and $|\Phi_{\rm C}^{\pm}\rangle$ and $|\Psi_{\rm C}^{\pm}\rangle$ are the Bell states of coherent states defined in Eqs. (2.36) and (2.37). Comparing Eqs. (4.4) and (4.7), we notice that in order to perform the logical Bell-state measurement to discriminate between four logical Bell states in Eqs. (4.5) and (4.6), one needs to perform two small Bell measurement units, i.e., one for $|\Phi_{\rm P}^{\pm}\rangle$ and $|\Psi_{\rm P}^{\pm}\rangle$ and the other is for $|\Phi_{\rm C}^{\pm}\rangle$ and $|\Psi_{\rm C}^{\pm}\rangle$ as shown in Eq. (4.7). Thus, the Bell-state measurement for the polarized single-photon states ($\rm B_P$ for modes a and b) and another Bell-state measurement for the coherent states ($\rm B_C$ for modes A and B) should be performed as illustrated in Fig. 10. For example, if $|\Phi_{\rm P}^{+}\rangle$ is detected by $\rm B_P$ and $|\Phi_{\rm C}^{+}\rangle$ is detected by $\rm B_C$, one can conclude that one of the logical Bell states, $|\Phi_{L}^{+}\rangle$, has been measured.

If we assume that available resources are linear optics elements and photodetectors (either single-photon detectors or number-resolving detectors), the

success probability of B_P is limited to 1/2 [24, 25] and the success probability of the B_C is $1-\exp(-2|\alpha|^2)$ [38]. A remarkable advantage of the scheme based on the hybrid qubits is that the whole teleportation process can be made successful as far as one of the two measurement elements, B_P or B_C, succeeds. To see this, consider the case of the measurement failure of B_P, which means that one cannot figure out whether the state was $|\Phi_P^+\rangle$ or $|\Phi_P^-\rangle$. The possible measurement outcomes according to the measurement result of B_C are then $|\Phi_P^+\rangle|\Phi_C^+\rangle$, $|\Phi_P^+\rangle|\Phi_C^-\rangle$, $|\Phi_P^-\rangle|\Psi_C^+\rangle$, or $|\Phi_P^-\rangle|\Psi_C^-\rangle$ as shown in Eq. (4.7). Thus, the success of the B_C measurement results in the success of the whole teleportation process. In the case of the measurement failure of B_C, in which one cannot figure out whether it was $|\Phi_C^+\rangle$ or $|\Psi_C^+\rangle$, the possible measurement outcomes according to the measurement result of B_P are $|\Phi_P^+\rangle|\Phi_C^+\rangle$, $|\Psi_P^+\rangle|\Phi_C^+\rangle$, $|\Phi_P^-\rangle|\Psi_C^+\rangle$, or $|\Psi_P^-\rangle|\Psi_C^+\rangle$ as shown in Eq. (4.7). Thus, the success of the B_P measurement results in the success of the whole teleportation process too. In this way, the success probability of teleportation of a hybrid qubit is $P_h = 1-\exp(-2|\alpha|^2)/2$ [38].

To complete the teleportation process, an appropriate Pauli operation ($\mathbb{1}$, $\hat{Z}$, $\hat{X}$, or $\hat{X}\hat{Z}$) should be applied according to the measurement result (U_S and U_C in Fig. 10). The Pauli operations for type-I hybrid qubits in the logical basis (4.1) can be done deterministically [38]. The Pauli X operation can be performed by applying a bit flip operation on each of the two modes. The implementations of a polarization rotator on the polarized single-photon states ($|+\rangle \leftrightarrow |-\rangle$), where $|\pm\rangle = (|H\rangle \pm |V\rangle)/\sqrt{2}$, and a π phase shifter on the co-

herent states ($|\alpha\rangle \leftrightarrow |-\alpha\rangle$) accomplish the Pauli X operation. The Pauli Z operation is performed by applying the π phase shift operation on the polarized single-photon states ($|\pm\rangle \rightarrow \pm|\pm\rangle$), and no operation is required on the coherent states.

The hybrid teleportation of type-II qubits can be carried out similarly to the case of type-I. The total product state of an unknown input state $|\phi\rangle$ and the channel state $|\Psi_{ch}\rangle$ can be written as Eq. (4.7) by replacing $|\Phi_{\rm P}^{\pm}\rangle$ and $|\Psi_{\rm P}^{\pm}\rangle$ with the Bell states of the vacuum and the single-photon states $|\Phi_{\rm V}^{\pm}\rangle$ and $|\Psi_{\rm V}^{\pm}\rangle$, respectively, which are defind in Eqs. (2.14) and (2.15). The Bell-state measurement for the vacuum and the single-photon states, $\rm B_V$, and the Bell-state measurement for the coherent states, $\rm B_C$, should then be performed.

The Pauli X operation for type-II hybrid qubits in the logical basis (4.1) can be implemented by acting the π phase shift on each of the two modes. However, the Pauli Z operation for type-II hybrid qubits cannot be performed deterministically. In order to perform the Pauli Z operation for type-II hybrid qubits, one needs a bit flip between $|0\rangle$ and $|1\rangle$ (i.e., $|0\rangle \leftrightarrow |1\rangle$) for the vacuum and the single-photon states or a sign flip for the coherent states ($|\pm\alpha\rangle \rightarrow \pm|\pm\alpha\rangle$) which can be implemented non-deterministically [17, 32]. One simple working solution is to "logically relabel" the vacuum and the single photon, $|0\rangle$ and $|1\rangle$, whenever it is necessary. In other words, we know that $|0\rangle$ and $|1\rangle$ remain unaltered, whenever they should be altered, so that it can be logically corrected at the final measurement stage. Under the assumption above, the success probability of quantum teleportation for type-II hybrid qubits is the

same to that for type-I qubits $P_h = 1 - \exp(-2|\alpha|^2)/2$.

4.2.3 Generation scheme for the channel state of type-II hybrid qubits

The channel state $|\Psi_{ch}\rangle$ for the quantum teleportation of the type-I hybrid qubits can be generated using two hybrid pairs [38],

$$|H\rangle|\sqrt{2}\alpha\rangle + |V\rangle|-\sqrt{2}\alpha\rangle. \tag{4.8}$$

Similarly, one can generate the channel state of the type-II hybrid qubits using two resource states,

$$|+\rangle|\sqrt{2}\alpha\rangle + |-\rangle|-\sqrt{2}\alpha\rangle, \tag{4.9}$$

where $|\pm\rangle = (|0\rangle \pm |1\rangle)/\sqrt{2}$, which was experimentally demonstrated recently [40] and the Bell-state measurement of the coherent states, $\mathrm{B_C}$. The resource states can be transformed to

$$|+\rangle|\alpha\rangle|-\alpha\rangle + |-\rangle|-\alpha\rangle|\alpha\rangle = |0_L\rangle|-\alpha\rangle + |1_L\rangle|\alpha\rangle, \tag{4.10}$$

by applying the 50:50 beam splitter on the coherent states. To perform the $\mathrm{B_C}$ measurement on these states, one of the coherent states of each state are

mixed by a 50:50 beam splitter, such that the total state evolves as

$$
\begin{aligned}
&(|0_L\rangle|-\alpha\rangle+|1_L\rangle|\alpha\rangle)(|0_L\rangle|-\alpha\rangle+|1_L\rangle|\alpha\rangle)\\
&\xrightarrow{BS}(|0_L\rangle|0_L\rangle+|1_L\rangle|1_L\rangle)\frac{1}{2N_\alpha^+}|\text{even}\rangle|0\rangle\\
&\quad-(|0_L\rangle|0_L\rangle-|1_L\rangle|1_L\rangle)\frac{1}{2N_\alpha^-}|\text{odd}\rangle|0\rangle\\
&\quad+(|0_L\rangle|1_L\rangle+|1_L\rangle|0_L\rangle)\frac{1}{2N_\alpha^+}|0\rangle|\text{even}\rangle\\
&\quad+(|0_L\rangle|1_L\rangle-|1_L\rangle|0_L\rangle)\frac{1}{2N_\alpha^-}|0\rangle|\text{odd}\rangle. \qquad (4.11)
\end{aligned}
$$

After the measurement of two photon-number-resolving detectors, the possible obtained states are $|0_L\rangle|0_L\rangle \pm |1_L\rangle|1_L\rangle$ and $|0_L\rangle|1_L\rangle \pm |1_L\rangle|0_L\rangle$. The latter states can be transformed to the former by applying the Pauli X operation on one of the logical qubits. Therefore, the channel state $|0_L\rangle|0_L\rangle + |1_L\rangle|1_L\rangle$ is generated with success probability $[1-\exp(-2|\alpha|^2)]^2/2$. We note that the state $|0_L\rangle|0_L\rangle - |1_L\rangle|1_L\rangle$ can also be used as a channel state. The only change caused by using the channel state $|0_L\rangle|0_L\rangle - |1_L\rangle|1_L\rangle$ instead of $|0_L\rangle|0_L\rangle + |1_L\rangle|1_L\rangle$ for the quantum teleportation is that the appropriate unitary transformations which are required in the last step of the teleportation process are switched by the amount of the Pauli Z operation ($\mathbb{1} \leftrightarrow \hat{Z}$, $\hat{X} \leftrightarrow \hat{X}\hat{Z}$).

4.3 Quantum teleportation for hybrid qubits under photon losses

In an ideal situation, quantum teleportation can be carried out with the unit success probability and the teleported state should be exactly the same to the input state. However, in realistic implementations, there are factors that reduce the success probability and the teleportation fidelity. Here, we consider two major such factors. One is inefficiency of the Bell-state measurement, and the other is photon losses in the quantum channel as shown in Fig. 10. In the following subsections, we will calculate and compare the fidelities between the input and the output states and the success probabilities of teleportation for two different types of hybrid qubits.

4.3.1 Teleportation of type-I hybrid qubits

The time evolution of density operator ρ under photon losses is given in Eq. (3.2). We assume that each mode of the channel state $|\Psi_{ch}\rangle$ suffers the same decoherence rate characterized by γ. The entangled channel of the type-I hybrid qubits at time τ under the above assumption is obtained using Eq. (3.2)

as

$$\begin{aligned}\rho_{\mathrm{I}}^{ch}(\tau) = \frac{1}{2}\Big\{ & \left[\left(t^2|+\rangle\langle+| + r^2|0\rangle\langle 0|\right) \otimes |t\alpha\rangle\langle t\alpha|\right]^{\otimes 2} \\ & + \left[\left(t^2|-\rangle\langle-| + r^2|0\rangle\langle 0|\right) \otimes |-t\alpha\rangle\langle -t\alpha|\right]^{\otimes 2} \\ & + \left[t^2 e^{-2|\alpha|^2 r^2}|+\rangle\langle-| \otimes |t\alpha\rangle\langle -t\alpha|\right]^{\otimes 2} \\ & + \left[t^2 e^{-2|\alpha|^2 r^2}|-\rangle\langle+| \otimes |-t\alpha\rangle\langle t\alpha|\right]^{\otimes 2}\Big\}, \end{aligned} \tag{4.12}$$

where $|\pm\rangle = (|H\rangle \pm |V\rangle)/\sqrt{2}$, $t = e^{-\gamma\tau/2}$, $r = \sqrt{1-e^{-\gamma\tau}}$, and $[\cdot]^{\otimes 2}$ means the direct product of same states. The parameter r containing both the real time τ and the decoherence rate γ will be used as the normalized time. As we see in Eq. (4.12), coherent-state qubits not only lose their relative phase information but also undergo amplitude damping by photon losses. However, we know the value of the interaction time τ, and we can use $|\pm t\alpha\rangle$ as a dynamic qubit basis in order to reflect the amplitude damping as suggested in Ref. [30]. The Bell states of coherent states using the dynamic qubit basis, $|\Phi_\alpha^{\pm}(\tau)\rangle$ and $|\Psi_\alpha^{\pm}(\tau)\rangle$, are defined in Eqs. (3.21) and (3.22). Adopting this, we define a dynamic orthonormal basis of optical hybrid qubits as

$$\{|0_L(\tau)\rangle = |+\rangle|t\alpha\rangle, |1_L(\tau)\rangle = |-\rangle|-t\alpha\rangle\}, \tag{4.13}$$

where $|\pm\rangle = (|H\rangle \pm |V\rangle)/\sqrt{2}$ and an unknown hybrid qubit which Alice wants to teleport as

$$|\phi(\tau)\rangle = \mu|0_L(\tau)\rangle + \nu|1_L(\tau)\rangle, \tag{4.14}$$

where $\mu = \cos(u/2)$ and $\nu = e^{iv}\sin(u/2)$. The logical Bell-state measurement should then be taken on the input state $|\phi(\tau)\rangle$ and one part of the decohered channel state $\rho_{\rm I}^{ch}(\tau)$. The Bell-state measurement for the polarized single-photon states, B_P, and that of the coherent states, B_C, are taken [38]. The B_C measurement is represented by the projection operators:

$$O_1 = \sum_{n=1}^{\infty} |2n\rangle_A\langle 2n| \otimes |0\rangle_B\langle 0|, \tag{4.15}$$

$$O_2 = \sum_{n=1}^{\infty} |2n-1\rangle_A\langle 2n-1| \otimes |0\rangle_B\langle 0|, \tag{4.16}$$

$$O_3 = \sum_{n=1}^{\infty} |0\rangle_A\langle 0| \otimes |2n\rangle_B\langle 2n|, \tag{4.17}$$

$$O_4 = \sum_{n=1}^{\infty} |0\rangle_A\langle 0| \otimes |2n-1\rangle_B\langle 2n-1|, \tag{4.18}$$

$$O_{\rm e} = |0\rangle_A\langle 0| \otimes |0\rangle_B\langle 0|, \tag{4.19}$$

where subscripts 1, 2, 3 and 4 correspond to Φ_C^+, Φ_C^-, Ψ_C^+ and Ψ_C^-, respectively, while $O_{\rm e}$ represents the measurement failure for which both the detectors do not register any photon. The B_P measurement is represented by

following projection operators,

$$M_1 = |HV\rangle_a\langle HV| \otimes |0\rangle_b\langle 0| + |0\rangle_a\langle 0| \otimes |HV\rangle_b\langle HV|, \tag{4.20}$$

$$M_2 = |H\rangle_a\langle H| \otimes |V\rangle_b\langle V| + |V\rangle_a\langle V| \otimes |H\rangle_b\langle H|, \tag{4.21}$$

$$\begin{aligned} M_{\mathrm{e}} = {} & |HH\rangle_a\langle HH| \otimes |0\rangle_b\langle 0| + |0\rangle_a\langle 0| \otimes |HH\rangle_b\langle HH| \\ & + |VV\rangle_a\langle VV| \otimes |0\rangle_b\langle 0| + |0\rangle_a\langle 0| \otimes |VV\rangle_b\langle VV|, \end{aligned} \tag{4.22}$$

where M_1 and M_2 correspond to Ψ_{P}^{+} and Ψ_{P}^{-}, respectively, while M_{e} represents a measurement failure. The teleportation process will be successful unless both $\mathrm{B_C}$ and $\mathrm{B_P}$ fail.

The unnormalized output state after measurement outcome $M_i \otimes O_j$ is obtained as

$$\rho_{\mathrm{I}}^{i,j} = \mathrm{Tr}_{a,b,A,B}[(U_{a,b} \otimes U_{A,B})(|\phi(\tau)\rangle\langle\phi(\tau)| \otimes \rho_{\mathrm{I}}^{ch}(\tau))(U_{a,b}^{\dagger} \otimes U_{A,B}^{\dagger})(M_i \otimes O_j)], \tag{4.23}$$

where the partial trace is taken over Alice's modes a, b, A and B in Fig. 10. Finally, Bob should perform appropriate unitary operations ($\mathbb{1}$, $\hat{Z}$, $\hat{X}$, or $\hat{X}\hat{Z}$) according to Alice's measurement results. The details are as follows: $\mathbb{1}$ for $\rho_{\mathrm{I}}^{1,2}$ and $\rho_{\mathrm{I}}^{\mathrm{e},1}$, $\hat{Z}$ for $\rho_{\mathrm{I}}^{1,1}$, $\rho_{\mathrm{I}}^{1,\mathrm{e}}$ and $\rho_{\mathrm{I}}^{\mathrm{e},2}$, $\hat{X}$ for $\rho_{\mathrm{I}}^{2,4}$ and $\rho_{\mathrm{I}}^{\mathrm{e},3}$, and $\hat{X}\hat{Z}$ for $\rho_{\mathrm{I}}^{2,3}$, $\rho_{\mathrm{I}}^{2,\mathrm{e}}$ and $\rho_{\mathrm{I}}^{\mathrm{e},4}$.

The final teleported state is then

$$\begin{aligned}\rho_{\mathrm{I}}^{T}(\tau) = {} & |\mu|^2\left(t^2|+\rangle\langle+| + r^2|0\rangle\langle 0|\right)\otimes|t\alpha\rangle\langle t\alpha| \\ & + |\nu|^2\left(t^2|-\rangle\langle-| + r^2|0\rangle\langle 0|\right)\otimes|-t\alpha\rangle\langle -t\alpha| \\ & + t^2 e^{-4|\alpha|^2 r^2}\left(\mu\nu^*|+\rangle\langle-|\otimes|t\alpha\rangle\langle -t\alpha| + \mu^*\nu|-\rangle\langle+|\otimes|-t\alpha\rangle\langle t\alpha|\right),\end{aligned} \tag{4.24}$$

regardless of the outcomes of the Bell-state measurements. The success probability is

$$\begin{aligned}P_{\mathrm{I}}(\tau) &= \sum_{j=1}^{2}\mathrm{Tr}_{c,C}[\rho_{\mathrm{I}}^{1,j}] + \sum_{j=3}^{4}\mathrm{Tr}_{c,C}[\rho_{\mathrm{I}}^{2,j}] + \sum_{i=1}^{2}\mathrm{Tr}_{c,C}[\rho_{\mathrm{I}}^{i,\mathrm{e}}] + \sum_{j=1}^{4}\mathrm{Tr}_{c,C}[\rho_{\mathrm{I}}^{\mathrm{e},j}] \\ &= t^2\left(1-\frac{1}{2}e^{-2|\alpha|^2 t^2}\right),\end{aligned} \tag{4.25}$$

where the trace was taken over for Bob's part. The average fidelity between the input state $|\phi(\tau)\rangle$ and the teleported state $\rho_{\mathrm{I}}^{T}(\tau)$ is

$$F_{\mathrm{I}}(\tau) = \frac{1}{4\pi}\int_0^{2\pi}\int_0^{\pi}\langle\phi(\tau)|\rho_{\mathrm{I}}^{T}(\tau)|\phi(\tau)\rangle\sin u\,\mathrm{d}u\mathrm{d}v = \frac{1}{3}t^2\left(2+e^{-4|\alpha|^2 r^2}\right). \tag{4.26}$$

The average is taken over in the Bloch sphere of all possible input states $|\phi(\tau)\rangle = \cos(u/2)|0_L(\tau)\rangle + e^{iv}\sin(u/2)|1_L(\tau)\rangle$ to be teleported. The results of the average fidelity and success probability are plotted in Fig. 11.

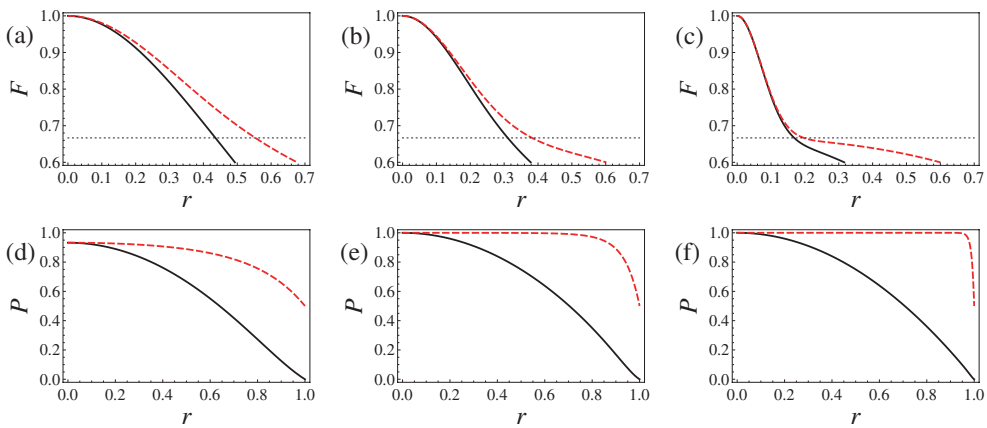

Figure 11: (a)-(c) Average fidelities and (d)-(f) average success probabilities of the type-I hybrid qubits (solid curves) and the type-II hybrid qubits (dashed curves) against the normalized time r. The horizontal dotted lines indicate classical limit, 2/3, which can be achieved by using a separable teleportation channel. Graphs are plotted with various values of amplitude α of coherent states as $|\alpha| = 1$ for (a) and (d), $|\alpha| = 2$ for (b) and (e), and $|\alpha| = 5$ for (c) and (f).

4.3.2 Teleportation of type-II hybrid qubits

We consider quantum teleportation of type-II hybrid qubits over a lossy environment. We assume that each mode of the channel state $|\Psi_{ch}\rangle$ suffers the same decoherence rate γ as before. The entangled channel at time τ under above assumption is obtained using Eq. (3.2) as

$$\rho_{\rm II}^{ch}(\tau) = \frac{1}{2}\Bigg\{ \left[\rho_{++}\otimes|t\alpha\rangle\langle t\alpha|\right]^{\otimes 2} + \left[\rho_{--}\otimes|-t\alpha\rangle\langle -t\alpha|\right]^{\otimes 2} + \left[e^{-2|\alpha|^2 r^2}\rho_{+-}\otimes|t\alpha\rangle\langle -t\alpha|\right]^{\otimes 2} + \left[e^{-2|\alpha|^2 r^2}\rho_{-+}\otimes|-t\alpha\rangle\langle t\alpha|\right]^{\otimes 2}\Bigg\}, \tag{4.27}$$

where

$$\rho_{++} = \frac{1+t}{2}|+\rangle\langle +| + \frac{1-t}{2}|-\rangle\langle -| + \frac{r^2}{2}|+\rangle\langle -| + \frac{r^2}{2}|-\rangle\langle +|, \tag{4.28}$$

$$\rho_{--} = \frac{1-t}{2}|+\rangle\langle +| + \frac{1+t}{2}|-\rangle\langle -| + \frac{r^2}{2}|+\rangle\langle -| + \frac{r^2}{2}|-\rangle\langle +|, \tag{4.29}$$

$$\rho_{+-} = \frac{t^2+t}{2}|+\rangle\langle -| + \frac{t^2-t}{2}|-\rangle\langle +|, \tag{4.30}$$

$$\rho_{-+} = (\rho_{+-})^{\dagger}, \tag{4.31}$$

and $|\pm\rangle = (|0\rangle \pm |1\rangle)/\sqrt{2}$. As before, we use the dynamic qubit basis for coherent states and define the new orthonormal basis as Eq. (4.13), $|0_L(\tau)\rangle = |+\rangle|t\alpha\rangle$ and $|1_L(\tau)\rangle = |-\rangle|-t\alpha\rangle$, where $|\pm\rangle = (|0\rangle \pm |1\rangle)/\sqrt{2}$, and an unknown hybrid qubit which Alice wants to teleport as $|\phi(\tau)\rangle = \mu|0_L(\tau)\rangle +$

$\nu|1_L(\tau)\rangle$. The logical Bell-state measurement should be performed on the input state $|\phi(\tau)\rangle$ and one part of the decohered channel state $\rho_{\rm II}^{ch}(\tau)$. The Bell-state measurement for the vacuum and the single-photon states, $\mathrm{B_V}$, and that of the coherent states, $\mathrm{B_C}$, are taken. The projection operators of the $\mathrm{B_C}$ measurement are already introduced in Sec. 4.3.1. The $\mathrm{B_V}$ measurement is represented by following projection operators,

$$E_1 = |0\rangle_a\langle 0| \otimes |1\rangle_b\langle 1|, \tag{4.32}$$

$$E_2 = |1\rangle_a\langle 1| \otimes |0\rangle_b\langle 0|, \tag{4.33}$$

$$E_{\rm e} = |0\rangle_a\langle 0| \otimes |0\rangle_b\langle 0| + |0\rangle_a\langle 0| \otimes |2\rangle_b\langle 2| + |2\rangle_a\langle 2| \otimes |0\rangle_b\langle 0|, \tag{4.34}$$

where $\Psi_{\rm V}^+$ and $\Psi_{\rm V}^-$ correspond to E_1 and E_2, and $E_{\rm e}$ represents a measurement failure. The teleportation process will be successful unless both $\mathrm{B_C}$ and $\mathrm{B_V}$ fail.

The unnormalized state after measurement outcome $E_i \otimes O_j$ is obtained as

$$\rho_{\rm II}^{i,j} = \mathrm{Tr}_{a,b,A,B}[(U_{a,b} \otimes U_{A,B})(|\phi(\tau)\rangle\langle\phi(\tau)| \otimes \rho_{\rm II}^{ch}(\tau))(U_{a,b}^\dagger \otimes U_{A,B}^\dagger)(E_i \otimes O_j)]. \tag{4.35}$$

Bob should perform appropriate logical gate operations ($\mathbb{1}$, $\hat{Z}$, $\hat{X}$, or $\hat{X}\hat{Z}$) according to measurement results of Alice. The details are as follows: $\mathbb{1}$ for $\rho_{\rm II}^{1,2}$, $\rho_{\rm II}^{2,1}$ and $\rho_{\rm II}^{\rm e,1}$, $\hat{Z}$ for $\rho_{\rm II}^{1,1}$, $\rho_{\rm II}^{2,2}$, $\rho_{\rm II}^{\rm e,2}$ and $\rho_{\rm II}^{1,\rm e}$, $\hat{X}$ for $\rho_{\rm II}^{1,3}$, $\rho_{\rm II}^{2,4}$ and $\rho_{\rm II}^{\rm e,3}$, and $\hat{X}\hat{Z}$

for $\rho_{\rm II}^{1,4}$, $\rho_{\rm II}^{2,3}$, $\rho_{\rm II}^{\rm e,4}$ and $\rho_{\rm II}^{2,\rm e}$. As discussed in Sec. 4.2.2, we assume that when the Pauli Z operation is necessary to complete the teleportation process, we do not apply it directly on the output but rather logically relabel $|0\rangle$ and $|1\rangle$.

The final teleported states after applying appropriate unitary transforms are different from each other according to the Bell-state measurement results. We present all possible teleported states (ρ_i^T), their probabilities (p_i) of obtaining such particular outcomes, and fidelities (f_i) with the input state $|\phi(\tau)\rangle$ in Sec. 4.3.3. Here we consider the average fidelity and the average success probability as

$$F_{\rm II}(\tau) = \frac{1}{4\pi}\int_0^{2\pi}\int_0^{\pi}\frac{\sum_i p_i f_i}{\sum_i p_i}\sin u\,{\rm d}u{\rm d}v, \tag{4.36}$$

$$P_{\rm II}(\tau) = \frac{1}{4\pi}\int_0^{2\pi}\int_0^{\pi}\sum_i p_i \sin u\,{\rm d}u{\rm d}v, \tag{4.37}$$

where the average is taken for all possible input states $|\phi(\tau)\rangle$ to be teleported and the summations run over 1 to 5. It is difficult to perform the integration in Eq. (4.36) in an analytical way because of the summation in the denominator, and we obtain the average fidelity $F_{\rm II}(\tau)$ numerically using MATHEMATICA. The average success probability in Eq. (4.37) is obtained as $P_{\rm II}(\tau) = 1 - \exp(-2|\alpha|^2 t^2)/2$; as one can see, the overall factor of t^2 in Eq. (4.25) is not here. While a qubit of the vacuum and the single photon in a type-II hybrid qubit after photon loss still remain in the logical qubit space, a polarized single-photon qubit in type-I hybrid qubit evolve out of the logical

qubit space due to the addition of the vacuum element under photon loss effects. Such a difference between type-I and type-II qubits makes the drop of the factor t^2.

We plot the average fidelity and the average success probability in Fig. 11. We also compare these results with the results obtained with the type-I qubits in Sec. 4.3.1. Our results in Fig. 11 clearly show that the average fidelity and the average success probability for type-II are always higher than those of type-I. Again, this can be attributed to the difference in the decoherence mechanism that a qubit of the vacuum and the single photon (type-II) remains in the qubit space under photon loss effects, while a polarized single-photon qubit (type-I) gets out of the qubit space.

4.3.3 The final teleported states of type-II hybrid qubits

In this subsection we present all possible teleported states, their probabilities of obtaining such particular outcomes and fidelities with the input state $|\phi(\tau)\rangle$ for the teleportation of type-II hybrid qubits. All the listed states are the final teleported states on which appropriate unitary transforms are applied. If the measurement results are revealed as $E_1 \otimes O_2$, $E_1 \otimes O_3$, $E_2 \otimes O_1$ and $E_2 \otimes O_4$, the final teleported states are

$$\begin{aligned}\rho_1^T(\tau) = {} & |\mu|^2 \rho_{++} \otimes |t\alpha\rangle\langle t\alpha| + |\nu|^2 \rho_{--} \otimes |-t\alpha\rangle\langle -t\alpha| \\ & + te^{-4|\alpha|^2 r^2} \left(\mu\nu^* \rho_{+-} \otimes |t\alpha\rangle\langle -t\alpha| + \mu^* \nu \rho_{-+} \otimes |-t\alpha\rangle\langle t\alpha|\right), \quad (4.38)\end{aligned}$$

with the probability

$$\begin{aligned} p_1(\tau) &= \mathrm{Tr}_{c,C}[\rho_{\mathrm{II}}^{1,2}] + \mathrm{Tr}_{c,C}[\rho_{\mathrm{II}}^{1,3}] + \mathrm{Tr}_{c,C}[\rho_{\mathrm{II}}^{2,1}] + \mathrm{Tr}_{c,C}[\rho_{\mathrm{II}}^{2,4}] \\ &= \frac{1}{4}\left(1 - e^{-2|\alpha|^2 t^2}\right)\left(1 + te^{-2|\alpha|^2 t^2}\right). \end{aligned} \tag{4.39}$$

Their fidelities with the input state $|\phi(\tau)\rangle$ are calculated as

$$\begin{aligned} f_1(\tau) = (|\mu|^4 + |\nu|^4)\frac{1+t}{2} + 2|\mu|^2|\nu|^2\left(\frac{1-t}{2}e^{-4|\alpha|^2 t^2} + t\frac{t^2+t}{2}e^{-4|\alpha|^2 r^2}\right) \\ + \left(\mu^2\nu^{*2} + \mu^{*2}\nu^2\right)t\frac{t^2-t}{2}e^{-4|\alpha|^2} + (\mu\nu^* + \mu^*\nu)\frac{r^2}{2}e^{-2|\alpha|^2 t^2}. \end{aligned} \tag{4.40}$$

If the measurement results are revealed as $E_1 \otimes O_1$, $E_1 \otimes O_4$, $E_2 \otimes O_2$ and $E_2 \otimes O_3$, the final teleported states are

$$\begin{aligned} \rho_2^T(\tau) = |\mu|^2\rho'_{++} \otimes |t\alpha\rangle\langle t\alpha| + |\nu|^2\rho'_{--} \otimes |-t\alpha\rangle\langle -t\alpha| \\ + te^{-4|\alpha|^2 r^2}\left(\mu\nu^*\rho_{+-} \otimes |t\alpha\rangle\langle -t\alpha| + \mu^*\nu\rho_{-+} \otimes |-t\alpha\rangle\langle t\alpha|\right), \end{aligned} \tag{4.41}$$

where

$$\rho'_{++} = \frac{1+t}{2}|+\rangle\langle +| + \frac{1-t}{2}|-\rangle\langle -| - \frac{r^2}{2}|+\rangle\langle -| - \frac{r^2}{2}|-\rangle\langle +|, \tag{4.42}$$

$$\rho'_{--} = \frac{1-t}{2}|+\rangle\langle +| + \frac{1+t}{2}|-\rangle\langle -| - \frac{r^2}{2}|+\rangle\langle -| - \frac{r^2}{2}|-\rangle\langle +|, \tag{4.43}$$

with the probability

$$\begin{aligned} p_2(\tau) &= \mathrm{Tr}_{c,C}[\rho_{\mathrm{II}}^{1,1}] + \mathrm{Tr}_{c,C}[\rho_{\mathrm{II}}^{1,4}] + \mathrm{Tr}_{c,C}[\rho_{\mathrm{II}}^{2,2}] + \mathrm{Tr}_{c,C}[\rho_{\mathrm{II}}^{2,3}] \\ &= \frac{1}{4}\left(1 - e^{-2|\alpha|^2 t^2}\right)\left(1 - t e^{-2|\alpha|^2 t^2}\right), \end{aligned} \tag{4.44}$$

and the fidelities are

$$\begin{aligned} f_2(\tau) = (|\mu|^4 + |\nu|^4)\frac{1+t}{2} + 2|\mu|^2|\nu|^2\left(\frac{1-t}{2}e^{-4|\alpha|^2 t^2} + t\frac{t^2+t}{2}e^{-4|\alpha|^2 r^2}\right) \\ + \left(\mu^2\nu^{*2} + \mu^{*2}\nu^2\right)t\frac{t^2-t}{2}e^{-4|\alpha|^2} - (\mu\nu^* + \mu^*\nu)\frac{r^2}{2}e^{-2|\alpha|^2 t^2}. \end{aligned} \tag{4.45}$$

If the measurement results are revealed as $E_{\mathrm{e}} \otimes O_1$ and $E_{\mathrm{e}} \otimes O_3$, the final teleported states are

$$\begin{aligned} \rho_3^T(\tau) = |\mu|^2 \rho_{++} \otimes |t\alpha\rangle\langle t\alpha| + |\nu|^2 \rho_{--} \otimes |-t\alpha\rangle\langle -t\alpha| \\ + t^2 e^{-4|\alpha|^2 r^2}\left(\mu\nu^* \rho_{+-} \otimes |t\alpha\rangle\langle -t\alpha| + \mu^*\nu \rho_{-+} \otimes |-t\alpha\rangle\langle t\alpha|\right), \end{aligned} \tag{4.46}$$

with the probability

$$p_3(\tau) = \mathrm{Tr}_{c,C}[\rho_{\mathrm{II}}^{\mathrm{e},1}] + \mathrm{Tr}_{c,C}[\rho_{\mathrm{II}}^{\mathrm{e},3}] = \frac{1}{4}\left(1 - e^{-2|\alpha|^2 t^2}\right)^2, \tag{4.47}$$

and the fidelities are

$$f_3(\tau) = (|\mu|^4 + |\nu|^4)\frac{1+t}{2} + 2|\mu|^2|\nu|^2\left(\frac{1-t}{2}e^{-4|\alpha|^2t^2} + t^2\frac{t^2+t}{2}e^{-4|\alpha|^2r^2}\right) + \left(\mu^2\nu^{*2} + \mu^{*2}\nu^2\right)t^2\frac{t^2-t}{2}e^{-4|\alpha|^2} + (\mu\nu^* + \mu^*\nu)\frac{r^2}{2}e^{-2|\alpha|^2t^2}. \quad (4.48)$$

If the measurement results are revealed as $E_e \otimes O_2$ and $E_e \otimes O_4$, the final teleported states are

$$\rho_4^T(\tau) = |\mu|^2\rho'_{++} \otimes |t\alpha\rangle\langle t\alpha| + |\nu|^2\rho'_{--} \otimes |-t\alpha\rangle\langle -t\alpha| + t^2e^{-4|\alpha|^2r^2}\left(\mu\nu^*\rho_{+-} \otimes |t\alpha\rangle\langle -t\alpha| + \mu^*\nu\rho_{-+} \otimes |-t\alpha\rangle\langle t\alpha|\right), \quad (4.49)$$

with the probability

$$p_4(\tau) = \mathrm{Tr}_{c,C}[\rho_{\mathrm{II}}^{e,2}] + \mathrm{Tr}_{c,C}[\rho_{\mathrm{II}}^{e,4}] = \frac{1}{4}(1-e^{-2|\alpha|^2t^2})(1+e^{-2|\alpha|^2t^2}), \quad (4.50)$$

and the fidelities are

$$f_4(\tau) = (|\mu|^4 + |\nu|^4)\frac{1+t}{2} + 2|\mu|^2|\nu|^2\left(\frac{1-t}{2}e^{-4|\alpha|^2t^2} + t^2\frac{t^2+t}{2}e^{-4|\alpha|^2r^2}\right) + \left(\mu^2\nu^{*2} + \mu^{*2}\nu^2\right)t^2\frac{t^2-t}{2}e^{-4|\alpha|^2} - (\mu\nu^* + \mu^*\nu)\frac{r^2}{2}e^{-2|\alpha|^2t^2}. \quad (4.51)$$

Lastly, for the measurement results of $E_1 \otimes O_{\rm e}$ and $E_2 \otimes O_{\rm e}$, the final teleported states are

$$\begin{aligned}
\rho_5^T(\tau) = & \frac{1}{1-(\mu\nu^* + \mu^*\nu)r^2} \\
& \times \left\{ \left(|\mu|^2 \frac{1+t}{2} - \mu\nu^* \frac{r^2}{2} - \mu^*\nu \frac{r^2}{2} + |\nu|^2 \frac{1-t}{2} \right) \rho'_{++} \otimes |t\alpha\rangle\langle t\alpha| \right. \\
& + \left(|\mu|^2 \frac{1-t}{2} - \mu\nu^* \frac{r^2}{2} - \mu^*\nu \frac{r^2}{2} + |\nu|^2 \frac{1+t}{2} \right) \rho'_{--} \otimes |-t\alpha\rangle\langle -t\alpha| \\
& + e^{-4|\alpha|^2 r^2} \left[\left(\mu\nu^* \frac{t^2+t}{2} + \mu^*\nu \frac{t^2-t}{2} \right) \rho_{+-} \otimes |t\alpha\rangle\langle -t\alpha| \right. \\
& \left. \left. + \left(\mu\nu^* \frac{t^2-t}{2} + \mu^*\nu \frac{t^2+t}{2} \right) \rho_{-+} \otimes |-t\alpha\rangle\langle t\alpha| \right] \right\} \qquad (4.52)
\end{aligned}$$

with the probability

$$p_5(\tau) = {\rm Tr}_{c,C}[\rho_{\rm II}^{1,{\rm e}}] + {\rm Tr}_{c,C}[\rho_{\rm II}^{2,{\rm e}}] = \frac{1}{2} e^{-2|\alpha|^2 t^2} \left[1 - (\mu\nu^* + \mu^*\nu) r^2 \right], \qquad (4.53)$$

and the fidelities are

$$\begin{aligned}
& f_5(\tau) \\
& = \frac{1}{1-(\mu\nu^* + \mu^*\nu)r^2} \left\{ (|\mu|^4 + |\nu|^4) \left[\left(\frac{1+t}{2} \right)^2 + \left(\frac{1-t}{2} \right)^2 e^{-4|\alpha|^2 t^2} \right] \right. \\
& + 2|\mu|^2|\nu|^2 \left[\frac{r^2}{4} \left(1 + e^{-2|\alpha|^2 t^2} \right)^2 + \left(\frac{t^2+t}{2} \right)^2 e^{-4|\alpha|^2 r^2} + \left(\frac{t^2-t}{2} \right)^2 e^{-4|\alpha|^2} \right] \\
& + (\mu^2\nu^{*2} + \mu^{*2}\nu^2) \left[\frac{r^4}{2} e^{-2|\alpha|^2 t^2} + \left(\frac{t^2+t}{2} \right) \left(\frac{t^2-t}{2} \right) \left(e^{-4|\alpha|^2 r^2} + e^{-4|\alpha|^2} \right) \right] \\
& \left. - (\mu\nu^* + \mu^*\nu) \frac{r^2}{2} \left(1 + e^{-2|\alpha|^2 t^2} \right) \left(\frac{1+t}{2} + \frac{1-t}{2} e^{-2|\alpha|^2 t^2} \right) \right\}. \qquad (4.54)
\end{aligned}$$

4.4 Remarks

In this chapter, we have discussed two types of hybrid qubits for quantum teleportation. One is the hybrid of a polarized single-photon qubit and a coherent-state qubit (type-I), and the other is the hybrid of a qubit of the vacuum and the single-photon and a coherent-state qubit (type-II). Using these two different types of hybrid qubits, we have analyzed the performance of quantum teleportation taking into account both the success probability and output fidelity under the effects of photon losses on the hybrid entangled channels. We found that both the average fidelity and the success probability of teleportation using the type-II hybrid qubits are always higher than those of the type-I hybrid qubits. The reason for this result is that a type-II hybrid qubit always, even under the effects of photon losses, remains in the logical qubit space spanned by the vacuum and the single-photon states. On the other hand, the leakage from the logical qubit space possibly occurs for the type-I hybrid qubits under the photon loss effects, due to the addition of the vacuum element to the photon polarization states. This difference leads to such lower fidelity and success probability for the type-I hybrid qubits. Our results show that the type-II hybrid qubits employing the vacuum and the single-photon states in the single-photon part may be better candidates of hybrid teleportation over a lossy environment. Our result is consistent with the study of single-mode qubits in Chap. 3 where the qubits of the vacuum and the single photon were found to be more efficient than the polarized single-photon qubits for the di-

rect transmission and quantum teleportation.

For future studies, it will be worth investigating the performance of two different types of hybrid qubits in the implementation of scalable quantum computation. For this, there are additional important factors to consider such as error correction models and fault-tolerant limits under the photon losses as well as resource requirements [15]. The effects of photon losses on quantum computation using the type-I hybrid qubit were already studied in Ref. [38]. In a similar way, it may be possible to investigate fault-tolerant limits for the type-II hybrid qubit under the photon loss effects and compare the results with those obtained with type-I qubits. In order to analyze and compare their performance more faithfully, it may be necessary to identify an appropriate error correction model for the type-II hybrid qubits.

Chapter 5

Conclusion

When we transfer optical quantum information, there are many ways to encode quantum information in light quanta, photons. We have considered three major candidates for optical quantum information transfer, such as qubits using the vacuum and single-photon states, polarized single-photon qubits, and coherent-state qubits.

We have reviewed quantum teleportation schemes of these optical qubits. Fidelity and success probability were suggested as measures to quantify the efficiency of quantum teleportation. The implementations of the Bell-state measurements and Pauli operations for each optical qubits were represented. For qubits using the vacuum and single-photon states and polarized single-photon qubits, only two of the four Bell states can be unambiguously discriminated. The discrimination of all four Bell states of coherent states is possible with arbitrary high success probability by increasing the amplitude of coherent states. Deterministic Pauli operations are possible with polarized single-photon qubits, while it is not the case for qubits using the vacuum and single-photon states and coherent-state qubits.

We have compared quantum teleportation and direct transmission using three different types of optical qubits under photon loss effects. The merit of

quantum teleportation is the travel time of each qubit of the channel state is half of the travel time of a single qubit for direct transmission. On the other hand, quantum teleportation has a demerit that both qubits of the channel state undergo decoherence effects, whereas only a single qubit does so for direct transmission. With the merit and demerit, it is intriguing to ask which transfer protocol gives better performance. We have found that the fidelity of quantum teleportation is always higher than that of direct transmission for qubits using the vacuum and single-photon states, polarized single-photon qubits, and coherent-state qubits with small amplitudes. For the coherent-state qubits with large amplitudes, the fidelity of quantum teleportation is higher than that of the direct transmission only in strong decoherence regions.

We have also compared fidelities of three different types of optical qubits for each information transfer scheme. It was shown that qubits using the vacuum and single-photon states are the most robust ones against photon losses for both information transfer schemes. Coherent-state qubits with small amplitudes are more robust than polarized single-photon qubits, whereas coherent-state qubits with large amplitudes outperform polarized single-photon qubits only in strong decoherence regions.

By combining different types of optical qubits, we have designed two different types of optical hybrid qubits. One is the hybrid of a qubit of the vacuum and the single-photon and a coherent-state qubit, and the other is the hybrid of a polarized single-photon qubit and a coherent-state qubit. We have compared two different types of hybrid qubits for quantum teleportation under

photon loss effects. It was shown that the hybrid of a qubit of the vacuum and the single-photon and a coherent-state qubit gives higher fidelity and success probability than the hybrid of a polarized single-photon qubit and a coherent-state qubit.

Lastly, we hope this thesis can be of help to whom want to understand optical quantum teleportation and the effects of photon losses.

Bibliography

[1] B. Schumacher, "Quantum coding," Phys. Rev. A **51**, 2738 (1995).

[2] M. A. Nielsen and I. L. Chuang, *Quantum Computation and Quantum Information*, Cambridge University Press, Cambridge (2010).

[3] A. Einstein, B. Podolsky, and N. Rosen, "Can quantum-mechanical description of physical reality be considered complete?" Phys. Rev. **47**, 777 (1935).

[4] E. Schrödinger, "Die gegenwärtige situation in der quantenmechanik," Naturwissenschaften **23**, 807 (1935).

[5] R. P. Feynman, "Simulating physics with computers," Int. J. Theor. Phys. **21**, 467 (1982).

[6] P. W. Shor, "Algorithms for quantum computation: discrete logarithms and factoring," in *Proceedings of the 35th Annual Symposium on Foundations of Computer Science*, IEEE Press, Los Alamitos, p. 124 (1994).

[7] L. K. Grover, "A fast quantum mechanical algorithm for database search," in *Proceedings of the 28th Annual ACM Symposium on the Theory of Computing*, ACM Press, New York, p. 212, (1996).

[8] C. H. Bennett and G. Brassard, "Quantum cryptography: public key distribution and coin tossing," in *Proceedings of IEEE International Conference on Computers, Systems and Signal Processing*, IEEE Press, New York, p. 175, (1984).

[9] C. H. Bennett, G. Brassard, C. Crépeau, R. Jozsa, A. Peres, and W. K. Wootters, "Teleporting an unknown quantum state via dual classical and Einstein-Podolsky-Rosen channels," Phys. Rev. Lett. **70**, 1895 (1993).

[10] M. Żukowski, A. Zeilinger, M. A. Horne, and A. K. Ekert, "'Event-ready-detectors' Bell experiment via entanglement swapping," Phys. Rev. Lett. **71**, 4287 (1993).

[11] H.-J. Briegel, W. Dür, J. I. Cirac, and P. Zoller, "Quantum repeaters: the role of imperfect local operations in quantum communication," Phys. Rev. Lett. **81**, 5932 (1998).

[12] D. Gottesman and I. L. Chuang, "Demonstrating the viability of universal quantum computation using teleportation and single-qubit operations," Nature (London) **402**, 390 (1999).

[13] D. Bouwmeester, J.-W. Pan, K. Mattle, M. Eibl, H. Weinfurter, and A. Zeilinger, "Experimental quantum teleportation," Nature (London) **390**, 575 (1997).

[14] P. Kok, W. J. Munro, K. Nemoto, T. C. Ralph, J. P. Dowling, and G. J. Milburn, "Linear optical quantum computing with photonic qubits," Rev. Mod. Phys. **79**, 135 (2007).

[15] T. C. Ralph and G. J. Pryde, "Optical quantum computation," Prog. Opt. **54**, 209 (2010).

[16] E. Knill, R. Laflamme, and G. J. Milburn, "A scheme for efficient quantum computation with linear optics," Nature **409**, 46 (2001).

[17] A. P. Lund and T. C. Ralph, "Nondeterministic gates for photonic single-rail quantum logic," Phys. Rev. A **66**, 032307 (2002).

[18] H. Jeong and M. S. Kim, "Efficient quantum computation using coherent states," Phys. Rev. A **65**, 042305 (2002).

[19] T. C. Ralph, A. Gilchrist, G. J. Milburn, W. J. Munro, and S. Glancy, "Quantum computation with optical coherent states," Phys. Rev. A **68**, 042319 (2003).

[20] S. Popescu, "Bell's inequalities versus teleportation: what is nonlocality?" Phys. Rev. Lett. **72**, 797 (1994).

[21] S. Massar and S. Popescu, "Optimal extraction of information from finite quantum ensembles," Phys. Rev. Lett. **74**, 1259 (1995).

[22] N. Gisin, "Nonlocality criteria for quantum teleportation," Phys. Lett. A **210**, 157 (1996).

[23] H.-W. Lee and J. Kim, "Quantum teleportation and Bell's inequality using single-particle entanglement," Phys. Rev. A **63**, 012305 (2000).

[24] N. Lütkenhaus, J. Calsamiglia, and K.-A. Suominen, "Bell measurements for teleportation," Phys. Rev. A **59**, 3295 (1999).

[25] J. Calsamiglia and N. Lütkenhaus, "Maximum efficiency of a linear-optical Bell-state analyzer," Appl. Phys. B **72**, 67 (2001).

[26] J. L. Dodd, T. C. Ralph, and G. J. Milburn, "Experimental requirements for Grover's algorithm in optical quantum computation," Phys. Rev. A **68**, 042328 (2003).

[27] R. J. Glauber, "Coherent and incoherent states of the radiation field," Phys. Rev. **131**, 2766 (1963).

[28] K. E. Cahill and R. J. Glauber, "Ordered expansions in boson amplitude operators," Phys. Rev. **177**, 1857 (1969).

[29] H. Jeong and M. S. Kim, "Purification of entangled coherent states," Quantum Inf. Comput. **2**, 208 (2002).

[30] H. Jeong, M. S. Kim, and J. Lee, "Quantum-information processing for a coherent superposition state via a mixed entangled coherent channel," Phys. Rev. A **64**, 052308 (2001).

[31] Y. W. Cheong, H. Kim, and H.-W. Lee, "Near-complete teleportation of a superposed coherent state," Phys. Rev. A **70**, 032327 (2004).

[32] A. P. Lund, T. C. Ralph, and H. L. Haselgrove, "Fault-tolerant linear optical quantum computing with small-amplitude coherent states," Phys. Rev. Lett. **100**, 030503 (2008).

[33] D. Boschi, S. Branca, F. De Martini, L. Hardy, and S. Popescu, "Experimental realization of teleporting an unknown pure quantum state via dual classical and Einstein-Podolsky-Rosen channels," Phys. Rev. Lett. **80**, 1121 (1998).

[34] S. J. van Enk and O. Hirota, "Entangled coherent states: teleportation and decoherence," Phys. Rev. A **64**, 022313 (2001).

[35] J. I. Cirac, P. Zoller, H. J. Kimble, and H. Mabuchi, "Quantum state transfer and entanglement distribution among distant nodes in a quantum network," Phys. Rev. Lett. **78**, 3221 (1997).

[36] P. van Loock, "Optical hybrid approaches to quantum information," Laser Photonics Rev. **5**, 167 (2011).

[37] K. Park, S.-W. Lee, and H. Jeong, "Quantum teleportation between particlelike and fieldlike qubits using hybrid entanglement under decoherence effects," Phys. Rev. A **86**, 062301 (2012).

[38] S.-W. Lee and H. Jeong, "Near-deterministic quantum teleportation and resource-efficient quantum computation using linear optics and hybrid qubits," Phys. Rev. A **87**, 022326 (2013).

[39] H. Jeong, A. Zavatta, M. Kang, S.-W. Lee, L. S. Costanzo, S. Grandi, T. C. Ralph, and M. Bellini, "Generation of hybrid entanglement of light," Nat. Photonics **8**, 564 (2014).

[40] O. Morin, K. Huang, J. Liu, H. L. Jeannic, C. Fabre, and J. Laurat, "Remote creation of hybrid entanglement between particle-like and wave-like optical qubits," Nat. Photonics **8**, 570 (2014).

[41] M. Takeoka, M. Ban, and M. Sasaki, "Quantum channel of continuous variable teleportation and nonclassicality of quantum states," J. Opt. B: Quantum Semiclassical Opt. **4**, 114 (2002).

[42] S. L. Braunstein, and H. J. Kimble, "Teleportation of continuous quantum variables," Phys. Rev. Lett. **80**, 869 (1998).

[43] A. Furusawa, J. L. Sørensen, S. L. Braunstein, C. A. Fuchs, H. J. Kimble, and E. S. Polzik, "Unconditional quantum teleportation," Science **282**, 706 (1998).

[44] K. Park and H. Jeong, "Entangled coherent states versus entangled photon pairs for practical quantum-information processing," Phys. Rev. A **82**, 062325 (2010).

[45] E. Lombardi, F. Sciarrino, S. Popescu, and F. De Martini, "Teleportation of a vacuum–one-photon qubit," Phys. Rev. Lett. **88**, 070402 (2002).

[46] K. J. Resch, J. S. Lundeen, and A. M. Steinberg, "Quantum state preparation and conditional coherence," Phys. Rev. Lett. **88**, 113601 (2002).

[47] A. I. Lvovsky and J. Mlynek, "Quantum-optical catalysis: generating nonclassical states of light by means of linear optics," Phys. Rev. Lett. **88**, 250401 (2002).

[48] S. A. Babichev, B. Brezger, and A. I. Lvovsky, "Remote preparation of a single-mode photonic qubit by measuring field quadrature noise," Phys. Rev. Lett. **92**, 047903 (2004).

[49] W. H. Louisell, *Quantum Statistical Properties of Radiation*, Wiley, New York (1973).

[50] S. J. D. Phoenix, "Wave-packet evolution in the damped oscillator," Phys. Rev. A **41**, 5132 (1990).

[51] G. Björk, A. Laghaout, and U. L. Andersen, "Deterministic teleportation using single-photon entanglement as a resource," Phys. Rev. A **85**, 022316 (2012).

[52] J. S. Neergaard-Nielsen, B. M. Nielsen, C. Hettich, K. Mølmer, and E. S. Polzik, "Generation of a superposition of odd photon number states for quantum information networks," Phys. Rev. Lett. **97**, 083604 (2006).

[53] A. Ourjoumtsev, R. Tualle-Brouri, J. Laurat, and P. Grangier, "Generating optical Schrödinger kittens for quantum information processing," Science **312**, 83 (2006).

[54] A. Ourjoumtsev, H. Jeong, R. Tualle-Brouri, and P. Grangier, "Generation of optical 'Schrödinger cats' from photon number states," Nature **448**, 784 (2007).

[55] H. Takahashi, K. Wakui, S. Suzuki, M. Takeoka, K. Hayasaka, A. Furusawa, and M. Sasaki, "Generation of large-amplitude coherent-state superposition via ancilla-assisted photon subtraction," Phys. Rev. Lett. **101**, 233605 (2008).

[56] M. Sasaki, M. Takeoka, and H. Takahashi, "Temporally multiplexed superposition states of continuous variables," Phys. Rev. A **77**, 063840 (2008).

[57] M. Takeoka, H. Takahashi, and M. Sasaki, "Large-amplitude coherent-state superposition generated by a time-separated two-photon subtraction from a continuous-wave squeezed vacuum," Phys. Rev. A **77**, 062315 (2008).

[58] T. Gerrits, S. Glancy, T. S. Clement, B. Calkins, A. E. Lita, A. J. Miller, A. L. Migdall, S. W. Nam, R. P. Mirin, and E. Knill, "Generation of optical coherent-state superpositions by number-resolved photon subtraction from the squeezed vacuum," Phys. Rev. A **82**, 031802(R) (2010).

[59] J. S. Neergaard-Nielsen, M. Takeuchi, K. Wakui, H. Takahashi, K. Hayasaka, M. Takeoka, and M. Sasaki, "Optical continuous-variable qubit," Phys. Rev. Lett. **105**, 053602 (2010).

[60] A. P. Lund, H. Jeong, T. C. Ralph, and M. S. Kim, "Conditional production of superpositions of coherent states with inefficient photon detection," Phys. Rev. A **70**, 020101(R) (2004).

[61] H. Jeong, A. P. Lund, and T. C. Ralph, "Production of superpositions of coherent states in traveling optical fields with inefficient photon detection," Phys. Rev. A **72**, 013801 (2005).

[62] A. M. Lance, H. Jeong, N. B. Grosse, T. Symul, T. C. Ralph, and P. K. Lam, "Quantum-state engineering with continuous-variable postselection," Phys. Rev. A **73**, 041801(R) (2006).

[63] H. Jeong, A. M. Lance, N. B. Grosse, T. Symul, P. K. Lam, and T. C. Ralph, "Conditional quantum-state engineering using ancillary squeezed-vacuum states," Phys. Rev. A **74**, 033813 (2006).

[64] M. Dakna, T. Anhut, T. Opatrný, L. Knöll, and D.-G. Welsch, "Generating Schrödinger-cat-like states by means of conditional measurements on a beam splitter," Phys. Rev. A **55**, 3184 (1997).

[65] P. Marek, H. Jeong, and M. S. Kim, "Generating 'squeezed' superpositions of coherent states using photon addition and subtraction," Phys. Rev. A **78**, 063811 (2008).

[66] H. Jeong, W. Son, M. S. Kim, D. Ahn, and Č. Brukner, "Quantum nonlocality test for continuous-variable states with dichotomic observables," Phys. Rev. A. **67**, 012106 (2003).

[67] V. Scarani, H. Bechmann-Pasquinucci, N. J. Cerf, M. Dušek, N. Lütkenhaus, and M. Peev, "The security of practical quantum key distribution," Rev. Mod. Phys. **81**, 1301 (2009).

[68] A. Miranowicz, "Optical-state truncation and teleportation of qudits by conditional eight-port interferometry," J. Opt. B: Quantum Semiclassical Opt. **7**, 142 (2005).

[69] J. Kim, J. Lee, S.-W. Ji, H. Nha, P. M. Anisimov, and J. P. Dowling, "Coherent-state optical qudit cluster state generation and teleportation via homodyne detection," Opt. Commun. **337**, 79 (2015).

[70] S. Lloyd and S. L. Braunstein, "Quantum computation over continuous variables," Phys. Rev. Lett. **82**, 1784 (1999).

[71] S. Pirandola, J. Eisert, C. Weedbrook, A. Furusawa, and S. L. Braunstein, "Advances in quantum teleportation," Nat. Photonics **9**, 641 (2015).

[72] C. M. Dawson, H. L. Haselgrove, and M.A. Nielsen, "Noise thresholds for optical cluster-state quantum computation," Phys. Rev. A **73**, 052306 (2006).

[73] A. J. F. Hayes, H. L. Haselgrove, A. Gilchrist, and T. C. Ralph, "Fault tolerance in parity-state linear optical quantum computing," Phys. Rev. A **82**, 022323 (2010).

[74] W. P. Grice, "Arbitrarily complete Bell-state measurement using only linear optical elements," Phys. Rev. A **84**, 042331 (2011).

[75] H. A. Zaidi and P. van Loock, "Beating the one-half limit of ancilla-free linear optics bell measurements," Phys. Rev. Lett. **110**, 260501 (2013).

[76] F. Ewert and P. van Loock, "3/4-efficient bell measurement with passive linear optics and unentangled ancillae," Phys. Rev. Lett. **113**, 140403 (2014).

[77] S.-W. Lee, K. Park, T. C. Ralph, and H. Jeong, "Nearly deterministic Bell measurement for multiphoton qubits and its application to quantum information processing," Phys. Rev. Lett. **114**, 113603 (2015).

[78] S.-W. Lee, K. Park, T. C. Ralph, and H. Jeong, "Nearly deterministic Bell measurement with multiphoton entanglement for efficient quantum-information processing," Phys. Rev. A **92**, 052324 (2015).

[79] H. Kwon and H. Jeong, "Violation of the Bell–Clauser-Horne-Shimony-Holt inequality using imperfect photodetectors with optical hybrid states," Phys. Rev. A **88**, 052127 (2013).

[80] C. C. Gerry, "Generation of optical macroscopic quantum superposition states via state reduction with a Mach-Zehnder interferometer containing a Kerr medium," Phys. Rev. A **59**, 4095 (1999).

[81] H. Jeong, "Using weak nonlinearity under decoherence for macroscopic entanglement generation and quantum computation," Phys. Rev. A **72**, 034305 (2005).

[82] W. J. Munro, K. Nemoto, and T. P. Spiller, "Weak nonlinearities: a new route to optical quantum computation," New J. Phys. **7**, 137 (2005).

[83] J. H. Shapiro and M. Razavi, "Continuous-time cross-phase modulation and quantum computation," New J. Phys. **9**, 16 (2007).

[84] H. Kwon and H. Jeong, "Generation of hybrid entanglement between a single-photon polarization qubit and a coherent state," Phys. Rev. A **91**, 012340 (2015).

[85] D. F. Walls and G. J. Milburn, "Effect of dissipation on quantum coherence," Phys. Rev. A **31**, 2403 (1985).

[86] S. Oh, S. Lee, and H.-W. Lee, "Fidelity of quantum teleportation through noisy channels," Phys. Rev. A **66**, 022316 (2002).

[87] Z.-X. Man and Y.-J. Xia, "Quantum teleportation in a dissipative environment," Quantum Inf. Process. **11**, 1911 (2012).

[88] F. De Martini, "Amplification of quantum entanglement," Phys. Rev. Lett. **81**, 2842 (1998).

[89] F. De Martini, F. Sciarrino, and C. Vitelli, "Entanglement test on a microscopic-macroscopic system," Phys. Rev. Lett. **100**, 253601 (2008).

[90] P. Sekatski, B. Sanguinetti, E. Pomarico, N. Gisin, and C. Simon, "Cloning entangled photons to scales one can see," Phys. Rev. A **82**, 053814 (2010).

[91] P. Sekatski, N. Sangouard, M. Stobińska, F. Bussières, M. Afzelius, and N. Gisin, "Proposal for exploring macroscopic entanglement with a single photon and coherent states," Phys. Rev. A **86**, 060301(R) (2012).

[92] R. Ghobadi, A. Lvovsky, and C. Simon, "Creating and detecting micro-macro photon-number entanglement by amplifying and deamplifying a single-photon entangled state," Phys. Rev. Lett. **110**, 170406 (2013).

[93] N. Bruno, A. Martin, P. Sekatski, N. Sangouard, R. T. Thew, and N. Gisin, "Displacement of entanglement back and forth between the micro and macro domains," Nat. Phys. **9**, 545 (2013).

[94] A. I. Lvovsky, R. Ghobadi, A. Chandra, A. S. Prasad, and C. Simon, "Observation of micro-macro entanglement of light," Nat. Phys. **9**, 541 (2013).

[95] U. L. Andersen and J. S. Neergaard-Nielsen, "Heralded generation of a micro-macro entangled state," Phys. Rev. A **88**, 022337 (2013).

[96] Y.-B. Sheng, L. Zhou, and G.-L. Long, "Hybrid entanglement purification for quantum repeaters," Phys. Rev. A **88**, 022302 (2013).

[97] S. Takeda, T. Mizuta, M. Fuwa, P. van Loock, and A. Furusawa, "Deterministic quantum teleportation of photonic quantum bits by a hybrid technique," Nature (London) **500**, 315 (2013).

[98] U. L. Andersen, J. S. Neergaard-Nielsen, P. van Loock, and A. Furusawa, "Hybrid discrete-and continuous-variable quantum information," Nat. Phys. **11**, 713 (2015).

국문초록

본 학위 논문의 목적은 광학적 큐비트를 이용한 양자 텔레포테이션의 과정에서 일어나는 광자 손실의 영향을 살펴보는 것이다. 양자 텔레포테이션의 자원으로 사용되는 채널 상태는 멀리 떨어진 두 사람이 이를 나누어 갖는 과정에서 결깨짐 효과에 노출된다. 우리는 서로 다른 종류의 광학적 큐비트를 사용해가면서 양자 텔레포테이션이 광자 손실 효과에 노출될 때 그 성과를 분석하였다.

우리는 세 가지 종류의 서로 다른 광학적 큐비트를 도입하였다. 하나는 진공과 단일 광자 상태를 이용한 큐비트이고, 또 하나는 편광된 단일 광자 큐비트이며, 나머지 하나는 결맞음 상태 큐비트이다. 우리는 서로 다른 광학적 큐비트를 이용하여 광자 손실 효과가 일어날 때 양자 텔레포테이션과 직접 전송의 정보 전달 효율을 비교하였다. 진공과 단일 광자 상태를 이용한 큐비트와 편광된 단일 광자 큐비트를 사용할 때에는 양자 텔레포테이션이 직접 전송보다 항상 더 높은 효율을 나타내었다. 결맞음 상태 큐비트의 경우에는 양자 텔레포테이션이 직접 전송보다 더 높은 효율을 나타내는 영역이 결맞음 상태 큐비트의 크기에 따라 달라졌다. 우리는 또한 진공과 단일 광자 상태를 이용한 큐비트가 세 가지 종류의 서로 다른 광학적 큐비트 가운데 가장 효율적임을 보였다.

앞서 언급한 광학적 큐비트 외에도 두 가지 종류의 서로 다른 광학적 혼종 큐비트가 고려되었다. 그것들은 진공과 단일 광자 상태를 이용한 큐비트와 결맞음 상태 큐비트의 혼종, 그리고 편광된 단일 광자 큐비트와 결맞음

상태 큐비트의 혼종이다. 우리는 광자 손실 효과가 일어날 때 두 가지 종류의 서로 다른 혼종 큐비트를 이용한 양자 텔레포테이션을 비교하였다. 그 결과 진공과 단일 광자 상태를 이용한 큐비트와 결맞음 상태 큐비트의 혼종이 편광된 단일 광자 큐비트와 결맞음 상태 큐비트의 혼종보다 항상 높은 효율을 보이는 것으로 나타났다.

주요어 : 양자 텔레포테이션, 양자정보처리, 양자광학, 결깨짐
학번 : 2011-20399